IEEE Access
Multidisciplinary ⋮ Rapid Review ⋮ Open Access Journal

Received 11 May 2024, accepted 3 June 2024, date of publication 19 June 2024, date of current version 28 June 2024.

Digital Object Identifier 10.1109/ACCESS.2024.3416553

RESEARCH ARTICLE

Secrecy Rate Maximization for Active Reconfigurable Intelligent Surface Assisted MIMO Systems

BIN GAO[1,2], JINGRU ZHAO[1], SHIHAO YAN[3], (Senior Member, IEEE), AND SHAOZHANG XIAO[1]

[1]Faculty of Computer and Software Engineering, Huaiyin Institute of Technology, Huaian 223003, China
[2]Key Laboratory of Underwater Acoustic Signal Processing of Ministry of Education, Southeast University, Nanjing 210018, China
[3]School of Science, Edith Cowan University, Perth, WA 6027, Australia

Corresponding author: Bin Gao (feimaxiao123@gmail.com)

ABSTRACT Reconfigurable intelligent surface (RIS) is a promising technology for future 6G communications and has been used to enhance secrecy performance. However, the performance improvement is restricted by the ''double fading'' effect of the reflection channel link. To address this issue, we introduce an active RIS design, where the reflecting elements of RIS not only adjust the phase shift but also amplify the reflected signal through the amplifier integrated into its elements. To obtain a satisfactory solution to the non-convex problem resulting from this design, the penalty dual decomposition based alternating gradient projection (PDDAPG) method is proposed. We compare the proposed algorithm with decoupling-fraction-based alternating optimization (DFAO). Specifically, the complexity of the proposed algorithm grows linearly with the number of reflective units in the RIS, while the complexity of the benchmark algorithm increases with the power of 4.5 times the number of reflective units. To further address the quality of service (QoS) constraints regarding the information rate requirements of users, we apply the fractional programming (FP) method and the successive convex approximation (SCA) method to optimize the precoder of the base station (BS) and the active beamformers of the phase shifts. The simulation results have demonstrated the effectiveness of the proposed PDDAPG method. Moreover, the active RIS can effectively mitigate the influence of ''double fading'' effects and achieve higher energy efficiency (EE) compared to passive RIS.

INDEX TERMS Reconfigurable intelligent surface (RIS), active RIS, penalty dual decomposition, secrecy rate.

I. INTRODUCTION

Reconfigurable intelligent surface (RIS) is a two-dimensional plane composed of many low-cost passive reflecting elements. An intelligent controller can adjust the amplitudes or phase shifts of the incident signal of each reflection unit through an independent control link to reflect the signal in the required direction [1]. Through this method, RIS can reshape the wireless communication environment, enhance the signal power received by legitimate users, or reduce the signals of eavesdroppers, thereby increasing the channel capacity of the entire wireless communication system and strengthening the secrecy and confidentiality of signal transmission [2], [3], [4].

Physical layer security has also been an important issue in recent years and a lot of research effort on RIS-assisted secure communications has been dedicated to the secrecy performance [5], [6], [7], [8] and secrecy optimization enhancement [9], [10], [11]. Liang et al. [5] investigated the secrecy performance of a RIS-aided wireless communication system considering multiple legal users and one eavesdropping user. Wei et al. [6] analyze the secrecy performance of a RIS-aided communication system with multiple eavesdroppers. Kaveh et al. [7] explored the role of RIS on enhancing the secure performance of smart grid communications. Ghadi et al. [8] provided the

The associate editor coordinating the review of this manuscript and approving it for publication was Stefan Schwarz.

performance analysis of physical layer security in presence of the correlated channel model for legal-illegal user pairs. In [11], the authors investigated the issue of secrecy rate in RIS-assisted multiple-antenna wiretap channel (WTC) and proposed an iterative method based on the block successive maximization to enhance the secrecy rate by updating the input covariance matrix and phase shifts. In [12], the authors maximized the secrecy rate in a power-constrained RIS-assisted multiple-input single-output (MISO) system, subject to delay-limited quality-of-service (QoS) constraint, using an iterative method and block coordinate ascent method.

Numerical results demonstrate that for systems with strict delay requirements, large-sized RIS can alleviate the degradation in secrecy rate performance. However, having a large number of reflecting elements increases channel estimation overhead and power consumption, making the control of RIS more challenging. Therefore, the practical application of passive RIS in wireless systems may be limited. In addition, the reflected signal of RIS is transmitted through two paths, i.e., the base station (BS)-RIS path and RIS-User path. Due to this transmission mode, the signal received by the user is affected by the ''double fading'' effect, resulting in a potential decrease in the channel gain compared to the direct link [13]. To address this challenge, the concept of active RIS has been proposed [14], [15]. Unlike traditional passive RIS, active RIS can amplify the reflected signal through the amplifier integrated into its reflecting elements. Moreover, compared to traditional amplify-and-forward (AF) relays, active RIS utilizes low-power reflection-type amplifiers to directly reflect signals in full-duplex (FD) mode. This eliminates the need for energy-intensive radio frequency (RF) chains and avoids the ''double fading'' effect. Furthermore, AF under FD mode requires reducing self-interference with high hardware intricacy. In [14], the simulation results indicate that for sum-rate maximization, active RIS outperforms passive RIS under relatively high power conditions and with a moderate number of RIS elements. Especially, in [10], the problem of maximizing the sum rate in an active RIS-assisted communications system is considered, and the transmit beamforming of BS and the reflecting beamforming of RIS are jointly optimized by an algorithm based on decoupling fraction alternating optimization (DFAO) [16]. Noting that, after extending the DFAO method in [10] to a multiuser MISO secure communication system, the complexity of each iteration increases with the 4.5 power of the number of RIS tiles, which results in high CPU costs for large-scale systems. Based on deep learning (DL) techniques and taking the maximal transmission rate as the loss function, Zhang et al. [26] learned to approximate the beamforming vector by using a full-connected deep neural network (DNN). Hu et al. [27] investigated the joint optimization of BS precoder and beam selection via a deep Q-network (DQN) approach.

The algorithms used in the aforementioned literature either directly approximate non-convex problems to convex ones through convex-concave procedure (CCP) and then utilize CVX to obtain suboptimal solutions [20], or employ model-free reinforcement learning algorithms. Both approaches fail to fully exploit the specific structure of the problem and are prone to getting trapped in suboptimal local optima. In comparison, PDDAPG can leverage the specific network structure aided by RIS for communication and provide closed-form solutions for precoding gradients of both BS and RIS. With appropriate step size selection, the PDDAPG algorithm converges quickly. Moreover, PDDAPG can also serve as an optimization kernel extension for the deep unfolding model [29]. Deep unfolding employs deep neural networks to approximate suboptimal step size selection, thereby accelerating the convergence of the PDDAPG algorithm, thus demonstrating promising application prospects for PDDAPG.

As such, this paper proposes a novel active RIS-assisted design aimed at enhancing secure wireless transmission in multi-antenna systems. The main contributions of this paper are summarized as follows:

1) We initially focus on maximizing the total achievable secrecy rate for all users given a fixed base station and active RIS power budget. To address this joint design problem, we propose a low-complexity and effective alternating gradient projection method based on penalty dual decomposition and provide closed-form expressions for exact gradients and projections. Our proposed method can be proven to converge to the critical point of the problem considered, which is desirable for non-convex programs.
2) Secondly, considering different QoS requirements, we aim to maximize the total secrecy rate of the system while ensuring a certain QoS allocation among legitimate users. To achieve this, based on fractional programming and closed-form solution of the capacity gratitude of the eavesdropper, we propose a joint transmit beamforming and reflect precod+ing scheme to solve this problem.
3) Finally, we provide extensive simulation results to demonstrate the effectiveness of the proposed PDDAPG algorithm and the joint beamforming and precoding scheme. Compared to other existing methods, the proposed PDDAPG algorithm shows significant improvements in enhancing secrecy rate with significantly reduced computational complexity. For instance, compared to the DFAO method [10], the proposed PDDAPG method achieves a 21% secrecy rate gain. Additionally, the proposed joint beamforming and precoding scheme not only improves the system's secrecy rate but also effectively meets the QoS requirements of each legitimate user. Lastly but equally importantly, we demonstrate that proactive RIS can effectively counteract the ''double fading'' effect and achieve higher secure energy efficiency (EE) compared to passive RIS.

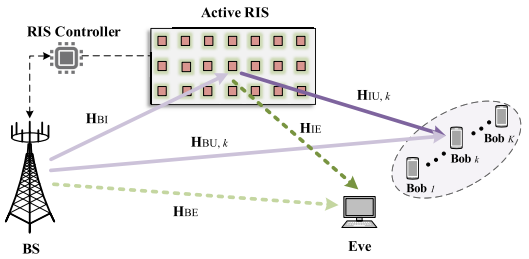

FIGURE 1. An active RIS-assisted multiuser MISO communication system.

II. SYSTEM MODEL AND PROBLEM FORMULATION

A. SYSTEM MODEL

We investigate an active RIS-assisted multiuser MISO system. As shown in Fig. 1, the system consists of a BS equipped with M antennas, an active RIS with N elements, a single-antenna eavesdropper (Eve), and K single-antenna legitimate users (Bobs). The intelligent controller working with the BS can dynamically modify the phase shift of each reflecting element. Let $\mathcal{K}$ be defined as the set $\{1, \cdots, K\}$, $\mathcal{M}$ be defined as the set $\{1, \cdots, M\}$, and $\mathcal{N}$ be defined as the set $\{1, \cdots, N\}$. These sets respectively represent the Bob set, the BS antenna set, and the RIS reflecting element set. The channels BS→RIS, RIS→Bob$_k$, BS→Bob$_k$, RIS→Eve, and BS→Eve are represented as $\mathbf{H}_{\mathrm{BI}} \in \mathbb{C}^{N\times M}$, $\mathbf{H}_{\mathrm{IU},k} \in \mathbb{C}^{1\times N}$, $\mathbf{H}_{\mathrm{BU},k} \in \mathbb{C}^{1\times M}$, $\mathbf{H}_{\mathrm{IE}} \in \mathbb{C}^{1\times N}$, and $\mathbf{H}_{\mathrm{BE}} \in \mathbb{C}^{1\times M}$, respectively. We assume that the full channel state information (CSI) of all channel links is known at the BS. Note that in the case where Eve is another user in the system but untrusted by Bobs, it is feasible to assume that $\mathbf{H}_{\mathrm{BE}}$ and $\mathbf{H}_{\mathrm{IE}}$ are known [17]. Accordingly, the transmitted signal from the BS can be expressed as

$$\mathbf{w} = \sum_{k\in\mathcal{K}} \mathbf{x}_k s_k, \tag{1}$$

where $\mathbf{x}_k \in \mathbb{C}^{M\times 1}$ is the beamforming vector for the Bob$_k$, s_k denotes the desired signal for the Bob$_k$ and follows $\mathbb{E}[|s_k|^2] = 1$, $\forall k \in \mathcal{K}$. We define $\mathbf{x} \triangleq [\mathbf{x}_1^T, \mathbf{x}_2^T, \cdots, \mathbf{x}_K^T]^T \in \mathbb{C}^{MK\times 1}$ to include the beamforming vector of all Bobs. The received signals at Bob$_k$ and at Eve are given by

$$\mathrm{y}_k = (\mathbf{H}_{\mathrm{BU},k} + \mathbf{H}_{\mathrm{IU},k}\Phi^H\mathbf{H}_{\mathrm{BI}})\mathbf{w} + \mathbf{H}_{\mathrm{IU},k}\Phi^H\mathbf{n}_{\mathbf{v}} + n_k, \tag{2}$$

$$\mathrm{y}_e = (\mathbf{H}_{\mathrm{BE}} + \mathbf{H}_{\mathrm{IE}}\Phi^H\mathbf{H}_{\mathrm{BI}})\mathbf{w} + \mathbf{H}_{\mathrm{IE}}\Phi^H\mathbf{n}_{\mathbf{v}} + n_e, \tag{3}$$

respectively, where $n_e \sim \mathcal{CN}(0, \sigma_e^2)$ and $n_k \sim \mathcal{CN}(0, \sigma^2)$ denote noise at Eve and Bob$_k$, respectively. $\Phi^H \triangleq \mathrm{diag}(\boldsymbol{\theta}) \in \mathbb{C}^{N\times N}$ is the reflection coefficient matrix of the active RIS, where $\boldsymbol{\theta} \triangleq [\theta_1, \theta_2, \cdots, \theta_N]^T \in \mathbb{C}^{N\times 1}$, $\theta_n = \beta_n e^{j\varphi_n}$, $\forall n \in \mathcal{N}$. Note that, $\varphi_n \in [0, 2\pi)$ and $\beta_n \in [0, \beta_{n,\max}]$ denote the phase shift and the amplification factor of the n-th reflecting element on the active RIS. In active RIS, due to the use of reflection-type amplifiers, there is usually $\beta_n > 1$. Let $\mathbf{n}_{\mathbf{v}} \sim \mathcal{CN}(0, \sigma_v^2\mathbf{I})$ represent the thermal noise produced in the RIS due to the presence of amplifiers. Different from passive RIS, the impact of this thermal noise cannot be ignored [10].

The signal-to-interference-plus-noise ratio (SINR) received at Bob$_k$ is calculated as follows

$$\mathrm{SINR}_k = \frac{\mathbf{x}_k^H\widetilde{\mathbf{H}}_{\mathrm{B},k}^H\widetilde{\mathbf{H}}_{\mathrm{B},k}\mathbf{x}_k}{\sum\limits_{i\in\mathcal{K},i\neq k}\widetilde{\mathbf{H}}_{\mathrm{B},k}\mathbf{x}_i(\widetilde{\mathbf{H}}_{\mathrm{B},k}\mathbf{x}_i)^H + \|\mathbf{H}_{\mathrm{IU},k}\Phi^H\|^2\sigma_v^2 + \sigma^2}, \tag{4}$$

where $\widetilde{\mathbf{H}}_{\mathrm{B},k} \triangleq (\mathbf{H}_{\mathrm{BU},k} + \mathbf{H}_{\mathrm{IU},k}\Phi^H\mathbf{H}_{\mathrm{BI}})$. The achievable rate of the Bob$_k$ can be expressed as $\mathrm{R}_k^{\mathrm{B}}(\mathbf{x}, \boldsymbol{\theta}) = \log_2(1 + \mathrm{SINR}_k)$.

The achievable rate of Eve attempt to eavesdrop on Bob$_k$'s signal can be expressed as

$$\mathrm{R}_k^{\mathrm{E}}(\mathbf{x}, \boldsymbol{\theta}) = \log_2\left(1 + \frac{\mathbf{x}_k^H\widetilde{\mathbf{H}}_{\mathrm{E}}^H\widetilde{\mathbf{H}}_{\mathrm{E}}\mathbf{x}_k}{\sum\limits_{i\in\mathcal{K},i\neq k}\widetilde{\mathbf{H}}_{\mathrm{E}}\mathbf{x}_i(\widetilde{\mathbf{H}}_{\mathrm{E}}\mathbf{x}_i)^H + \|\mathbf{H}_{\mathrm{IE}}\Phi^H\|^2\sigma_v^2 + \sigma_e^2}\right), \tag{5}$$

where $\widetilde{\mathbf{H}}_{\mathrm{E}} \triangleq (\mathbf{H}_{\mathrm{BE}} + \mathbf{H}_{\mathrm{IE}}\Phi^H\mathbf{H}_{\mathrm{BI}})$.

Thus, the secrecy rate between the BS and the Bob$_k$ can be expressed as

$$\mathrm{R}_k^{\mathrm{sec}}(\mathbf{x}, \boldsymbol{\theta}) = \left[\mathrm{R}_k^{\mathrm{B}}(\mathbf{x}, \boldsymbol{\theta}) - \mathrm{R}_k^{\mathrm{E}}(\mathbf{x}, \boldsymbol{\theta})\right]. \tag{6}$$

B. PROBLEM FORMULATION

Our objective is to iteratively approximate the maximum sum secrecy rate (SSR) by alternatively obtaining the optimal passive beamformer $\mathbf{x}$ and the active RIS beamforming matrix Φ^H. The optimization problem is formulated as

$$(\mathcal{P}1): \max_{\mathbf{x},\boldsymbol{\theta}} \left\{\mathrm{R}^{\mathrm{sec}}(\mathbf{x}, \boldsymbol{\theta}) \triangleq \sum_{k\in\mathcal{K}} \mathrm{R}_k^{\mathrm{sec}}(\mathbf{x}, \boldsymbol{\theta})\right\} \tag{7a}$$

$$\text{s.t.} \sum_{k\in\mathcal{K}} \|\Phi^H\mathbf{H}_{\mathrm{BI}}\mathbf{x}_k\|^2 + \|\Phi^H\|_F^2\sigma_v^2 \leq P_{\mathrm{A}}^{\max}, \tag{7b}$$

$$\|\mathbf{x}\|^2 \leq P_{\mathrm{BS}}^{\max}, \tag{7c}$$

$$|\boldsymbol{\theta}_n| \leq \beta_{n,\max}, \forall n \in \mathcal{N}, \tag{7d}$$

where $P_{\mathrm{A}}^{\max}$ and $P_{\mathrm{BS}}^{\max}$ represent the maximum reflect power of RIS and the maximum transmit power at BS, respectively. The total power consumption $P^{\max} = P_{\mathrm{A}}^{\max} + P_{\mathrm{BS}}^{\max}$.

III. PDD-BASED SOLUTION WITHOUT QOS CONSTRAINTS

Iterating to the optimal solution is extremely intractable due to the non-convex nature of both the objective function $(\mathcal{P}1)$ and the constraints (7b). For the optimization problem similar to the system composed of a multi-antenna BS, an active RIS, and multiple single-antenna users, [10] proposed an AO-based algorithm using a closed-form DFAO method [16]. Noting that the main idea of the closed-form DFAO method used in [10] is to first restate the objective function in a sum-of-ratio form using the Lagrangian dual transform, then apply the quadratic transform to the ratios, and finally optimize each variable in a closed-form alternating manner. This DFAO method has lower complexity but inferior

optimization performance compared to the direct DFAO method [16], resulting in poorer system performance in general. Furthermore, the DFAO method in [10], whose per-iteration complexity increases with the number of RIS tiles to the power of 4.5, is impractical for large-scale systems. Inspired by these shortcomings, we introduce a low-complexity and effective PDDAPG method to obtain a fixed solution for $(\mathcal{P}1)$.

To address the non-convex constraint in (7b), we apply the PDD method introduced in [18]. The main idea of the PDD method is to handle difficult coupled constraints through Lagrangian relaxation, then perform block decomposition on the resulting augmented Lagrangian function, and finally implement relaxed equality constraints with appropriate penalty parameters. Specifically, first, we define $h(\mathbf{x},\boldsymbol{\theta},P_{\mathrm{A}}^{\max},\varsigma)\triangleq\sum_{k\in\mathcal{K}}\|\Phi^H\mathbf{H}_{\mathrm{BI}}\mathbf{x}_k\|^2+\|\Phi^H\|_F^2\sigma_v^2-P_{\mathrm{A}}^{\max}+\varsigma$. Then the constraint (7b) is equivalent to $h(\mathbf{x},\boldsymbol{\theta},P_{\mathrm{A}}^{\max},\varsigma)=0$, $\varsigma\geqslant 0$. Next, we use the Lagrangian relaxation technique to handle the coupled constraints $h(\mathbf{x},\boldsymbol{\theta},P_{\mathrm{A}}^{\max},\varsigma)=0$, and correspondingly, we can obtain the augmented Lagrangian function for (7a):

$$\bar{\mathrm{R}}_{\xi,\omega}^{\mathrm{sec}}(\mathbf{x},\boldsymbol{\theta},\varsigma)\triangleq \mathrm{R}^{\mathrm{sec}}(\mathbf{x},\boldsymbol{\theta})-\xi h(\mathbf{x},\boldsymbol{\theta},P_{\mathrm{A}}^{\max},\varsigma)-\frac{\omega}{2}h^2(\mathbf{x},\boldsymbol{\theta},P_{\mathrm{A}}^{\max},\varsigma),\tag{8}$$

where ξ representing the Lagrangian multiplier associated with the constraint $h(\mathbf{x},\boldsymbol{\theta},P_{\mathrm{A}}^{\max},\varsigma)=0$ and ω representing the penalty parameter. The penalty parameter ω is used to adjust the value of ξ at each iteration step to ensure the constraints are satisfied. After ξ and ω are fixed, problem $(\mathcal{P}1)$ is transformed to:

$$(\mathcal{P}2):\quad \max_{\mathbf{x},\boldsymbol{\theta},\varsigma}\quad \bar{\mathrm{R}}_{\xi,\omega}^{\mathrm{sec}}(\mathbf{x},\boldsymbol{\theta},\varsigma)\tag{9a}$$

$$\text{s.t.}\quad \varsigma\geq 0,\ (7c),\ (7d).\tag{9b}$$

We establish the feasible region for the variable $\mathbf{x}$ as $\mathcal{X}$, which is defined as $\{\mathbf{x}\in\mathbb{C}^{MK\times 1},\|\mathbf{x}\|^2\leq P_{\mathrm{BS}}^{\max}\}$. Note that for the active RIS, there is no need for $\boldsymbol{\theta}$ to satisfy the unit modulus constraint $|\boldsymbol{\theta}_n|=1$. Thus, the feasible set for the variable $\boldsymbol{\theta}$ as Θ, and is defined as $\{\boldsymbol{\theta}\in\mathbb{C}^{N\times 1},|\boldsymbol{\theta}_n|\leq\beta_{n,\max},\forall n\in\mathcal{N}\}$. Due to the decoupling of optimization variables in $(\mathcal{P}2)$, we use the APG method to search for the stationary solution of $(\mathcal{P}2)$. The motivation behind the APG method is that the projection of the feasible set for a single variable can be expressed in closed form.

Below are the steps for applying the APG algorithm to iteratively approximate the optimal solution of problem $(\mathcal{P}2)$. Following **Algorithm 1** in line 5, we commence our movement from $\mathbf{x}^{n-1}$ by taking a step of size α^n along its gradient. We then project the resulting point (i.e., $\ddot{\mathbf{x}}^n\triangleq\mathbf{x}^{n-1}+\alpha^n\nabla_{\mathbf{x}}\bar{\mathrm{R}}_{\xi,\omega}^{\mathrm{sec}}(\mathbf{x}^{n-1},\boldsymbol{\theta}^{n-1},\varsigma^{n-1})$) onto $\mathcal{X}$, resulting in $\mathbf{x}^n$. In the same way, the line 6 moves along the gradient of $\boldsymbol{\theta}^{n-1}$ by the step size τ^n, and then projects the resulting point (i.e., $\ddot{\boldsymbol{\theta}}^n\triangleq\boldsymbol{\theta}^{n-1}+\tau^n\nabla_{\boldsymbol{\theta}}\bar{\mathrm{R}}_{\xi,\omega}^{\mathrm{sec}}(\mathbf{x}^n,\boldsymbol{\theta}^{n-1},\varsigma^{n-1})$) onto Θ to obtain $\boldsymbol{\theta}^n$. Following the update of $\mathbf{x}$ and $\boldsymbol{\theta}$ in **Algorithm 1**, we turn

Algorithm 1 Gradient Projection Algorithm for Solving $(\mathcal{P}2)$

1: **Input:** $\mathbf{x}^0,\boldsymbol{\theta}^0,\varsigma^0,\alpha^0,\tau^0,\xi,\omega>0,n\leftarrow 0$
2: Initialize $\mathbf{x}^0$ and $\boldsymbol{\theta}^0$
3: **repeat**
4: $n\leftarrow n+1$;
5: $\mathbf{x}^n=\Pi_{\mathcal{X}}(\ddot{\mathbf{x}}^n\triangleq\mathbf{x}^{n-1}+\alpha^n\nabla_{\mathbf{x}}\bar{\mathrm{R}}_{\xi,\omega}^{\mathrm{sec}}(\mathbf{x}^{n-1},\boldsymbol{\theta}^{n-1},\varsigma^{n-1}))$;
6: $\boldsymbol{\theta}^n=\Pi_{\Theta}(\ddot{\boldsymbol{\theta}}^n\triangleq\boldsymbol{\theta}^{n-1}+\tau^n\nabla_{\boldsymbol{\theta}}\bar{\mathrm{R}}_{\xi,\omega}^{\mathrm{sec}}(\mathbf{x}^n,\boldsymbol{\theta}^{n-1},\varsigma^{n-1}))$;
7: $\varsigma^n=\max\{0,P_{\mathrm{A}}^{\max}-\sum_{k\in\mathcal{K}}\|\mathrm{diag}(\boldsymbol{\theta}^n)\mathbf{H}_{\mathrm{BI}}\mathbf{x}_k^n\|^2-\|\mathrm{diag}(\boldsymbol{\theta}^n)\|_F^2\sigma_v^2\}$;
8: **until** *convergence*;
9: **Output:** $\mathbf{x}^n,\boldsymbol{\theta}^n,\varsigma^n$

to the optimization of ς in line 7. When $\mathbf{x}$ and $\boldsymbol{\theta}$ are fixed, the optimal solution of $(\mathcal{P}2)$ is simply given, that is, $\varsigma^n=\max\{0,P_{\mathrm{A}}^{\max}-\sum_{k\in\mathcal{K}}\|\mathrm{diag}(\boldsymbol{\theta}^n)\mathbf{H}_{\mathrm{BI}}\mathbf{x}_k^n\|^2-\|\mathrm{diag}(\boldsymbol{\theta}^n)\|_F^2\sigma_v^2\}$. Therefore, it is not necessary to project ς.

The next iterative values of α^n and τ^n can be acquired by *backtrackinglinesearchscheme* in each iteration. Specifically, we can set $\alpha^n=\alpha^{n-1}\zeta$, so that

$$\begin{aligned}\bar{\mathrm{R}}_{\xi,\omega}^{\mathrm{sec}}(\mathbf{x}^n,\boldsymbol{\theta}^{n-1},\varsigma^{n-1})\geq{}&\bar{\mathrm{R}}_{\xi,\omega}^{\mathrm{sec}}(\mathbf{x}^{n-1},\boldsymbol{\theta}^{n-1},\varsigma^{n-1})\\&+2\Re\{(\nabla_{\mathbf{x}}\bar{\mathrm{R}}_{\xi,\omega}^{\mathrm{sec}}(\mathbf{x}^{n-1},\boldsymbol{\theta}^{n-1},\varsigma^{n-1}))^H(\mathbf{x}^n-\mathbf{x}^{n-1})\}\\&-\frac{1}{\alpha^{n-1}\zeta}\|\mathbf{x}^n-\mathbf{x}^{n-1}\|^2,\end{aligned}\tag{10}$$

where $\zeta<1$. A similar strategy can be employed thereafter to obtain τ^n. Subsequently, we provide a comprehensive explanation of the two primary operations performed in **Algorithm 1**

1) Projection to sets $\mathcal{X}$ and Θ: The projection of $\ddot{\mathbf{x}}^n$ onto set $\mathcal{X}$ is given by

$$\Pi_{\mathcal{X}}(\ddot{\mathbf{x}}^n)=\frac{\sqrt{P_{\mathrm{BS}}^{\max}}\ddot{\mathbf{x}}^n}{\max\{\sqrt{P_{\mathrm{BS}}^{\max}},\|\ddot{\mathbf{x}}^n\|\}}.\tag{11}$$

The projection of $\ddot{\boldsymbol{\theta}}^n=[\ddot{\theta}_1^n,\ddot{\theta}_2^n,\ldots,\ddot{\theta}_N^n]^T$ onto set Θ is given by $\Pi_{\Theta}(\ddot{\boldsymbol{\theta}}^n)=[\bar{\theta}_1^n,\bar{\theta}_2^n,\ldots,\bar{\theta}_N^n]^T$, where for each $l\in\mathcal{N}$

$$\bar{\theta}_l^n=\begin{cases}(\ddot{\theta}_l^n/|\ddot{\theta}_l^n|)\beta_{l,\max} & ,\text{if}\quad |\ddot{\theta}_l^n|>\beta_{l,\max}\\ \ddot{\theta}_l^n & ,\text{otherwise.}\end{cases}\tag{12}$$

2) Gradient of $\bar{\mathrm{R}}_{\xi,\omega}^{\mathrm{sec}}(\mathbf{x},\boldsymbol{\theta},\varsigma)$ for $(\mathcal{P}2)$: The gradient of $\bar{\mathrm{R}}_{\xi,\omega}^{\mathrm{sec}}(\mathbf{x},\boldsymbol{\theta},\varsigma)$ with respect to $\mathbf{x}$ is defined as follows

$$\begin{aligned}\nabla_{\mathbf{x}}\bar{\mathrm{R}}_{\xi,\omega}^{\mathrm{sec}}(\mathbf{x},\boldsymbol{\theta},\varsigma)=[&(\nabla_{\mathbf{x}_1}\bar{\mathrm{R}}_{\xi,\omega}^{\mathrm{sec}}(\mathbf{x},\boldsymbol{\theta},\varsigma))^T,(\nabla_{\mathbf{x}_2}\bar{\mathrm{R}}_{\xi,\omega}^{\mathrm{sec}}(\mathbf{x},\boldsymbol{\theta},\varsigma))^T,\\&\ldots,(\nabla_{\mathbf{x}_K}\bar{\mathrm{R}}_{\xi,\omega}^{\mathrm{sec}}(\mathbf{x},\boldsymbol{\theta},\varsigma))^T]^T,\end{aligned}\tag{13}$$

where

$$\nabla_{\mathbf{x}_k}\bar{\mathrm{R}}_{\xi,\omega}^{\mathrm{sec}}(\mathbf{x},\boldsymbol{\theta},\varsigma)=\nabla_{\mathbf{x}_k}\mathrm{R}^{\mathrm{sec}}(\mathbf{x},\boldsymbol{\theta})-\left(\xi+\omega h(\mathbf{x},\boldsymbol{\theta},P_{\mathrm{A}}^{\max},\varsigma)\right)\mathbf{H}_{\mathrm{BI}}^H\Phi^H\Phi^H\mathbf{H}_{\mathrm{BI}}\mathbf{x}_k.$$

For convenience of expression, we define

$$B_k(\mathbf{x},\boldsymbol{\theta})=\sum_{i\in\mathcal{K},i\neq k}\widetilde{\mathbf{H}}_{\mathrm{B},k}\mathbf{x}_i(\widetilde{\mathbf{H}}_{\mathrm{B},k}\mathbf{x}_i)^H+\|\mathbf{H}_{\mathrm{IU},k}\Phi^H\|^2\sigma_v^2+\sigma^2$$

and

$$C_k(\mathbf{x},\boldsymbol{\theta}) = \sum_{i\in\mathcal{K},i\neq k} \widetilde{\mathbf{H}}_{\mathrm{E}}\mathbf{x}_i(\widetilde{\mathbf{H}}_{\mathrm{E}}\mathbf{x}_i)^H + \|\mathbf{H}_{\mathrm{IE}}\Phi^H\|^2\sigma_v^2 + \sigma_e^2.$$

The gradient of $\mathrm{R}^{\mathrm{sec}}(\mathbf{x},\boldsymbol{\theta})$ with respect to $\mathbf{x}_k$ is

$$\nabla_{\mathbf{x}_k}\mathrm{R}^{\mathrm{sec}}(\mathbf{x},\boldsymbol{\theta}) = \nabla_{\mathbf{x}_k}\mathrm{A1}(\mathbf{x},\boldsymbol{\theta}) - \nabla_{\mathbf{x}_k}\mathrm{A2}(\mathbf{x},\boldsymbol{\theta}), \tag{14}$$

where $\nabla_{\mathbf{x}_k}\mathrm{A1}(\mathbf{x},\boldsymbol{\theta})$ and $\nabla_{\mathbf{x}_k}\mathrm{A2}(\mathbf{x},\boldsymbol{\theta})$ are given by (15) and (16), as shown at the bottom of the next page, respectively.

The gradient of $\bar{\mathrm{R}}^{\mathrm{sec}}_{\xi,\omega}(\mathbf{x},\boldsymbol{\theta},\varsigma)$ with respect to $\boldsymbol{\theta}$ is

$$\nabla_{\boldsymbol{\theta}}\bar{\mathrm{R}}^{\mathrm{sec}}_{\xi,\omega}(\mathbf{x},\boldsymbol{\theta},\varsigma) = \nabla_{\boldsymbol{\theta}}\mathrm{R}^{\mathrm{sec}}(\mathbf{x},\boldsymbol{\theta}) - \left(\xi + \omega h(\mathbf{x},\boldsymbol{\theta},P_{\mathrm{A}}^{\max},\varsigma)\right) \times \left(\sum_{k\in\mathcal{K}} \mathrm{vec_d}\left(\Phi^H\mathbf{H}_{\mathrm{BI}}\mathbf{x}_k\mathbf{x}_k^H\mathbf{H}_{\mathrm{BI}}^H\right) + \boldsymbol{\theta}\sigma_v^2\right). \tag{17}$$

The gradient of $\mathrm{R}^{\mathrm{sec}}(\mathbf{x},\boldsymbol{\theta})$ with respect to $\boldsymbol{\theta}$ is

$$\nabla_{\boldsymbol{\theta}}\mathrm{R}^{\mathrm{sec}}(\mathbf{x},\boldsymbol{\theta}) = \sum_{k\in\mathcal{K}} \nabla_{\boldsymbol{\theta}}\mathrm{A1}k(\mathbf{x},\boldsymbol{\theta}) - \sum_{k\in\mathcal{K}} \nabla_{\boldsymbol{\theta}}\mathrm{A2}k(\mathbf{x},\boldsymbol{\theta}), \tag{18}$$

where

$$\nabla_{\boldsymbol{\theta}}\mathrm{A1}k(\mathbf{x},\boldsymbol{\theta}) = \frac{\nabla_{\boldsymbol{\theta}}\mathrm{M1}k(\mathbf{x},\boldsymbol{\theta})}{(1+\mathbf{x}_k^H\widetilde{\mathbf{H}}_{\mathrm{B},k}^H\widetilde{\mathbf{H}}_{\mathrm{B},k}\mathbf{x}_k/B_k(\mathbf{x},\boldsymbol{\theta}))\ln 2}, \tag{19}$$

$$\nabla_{\boldsymbol{\theta}}\mathrm{A2}k(\mathbf{x},\boldsymbol{\theta})\frac{\nabla_{\boldsymbol{\theta}}\mathrm{M2}k(\mathbf{x},\boldsymbol{\theta})}{(1+\mathbf{x}_k^H\widetilde{\mathbf{H}}_{\mathrm{E}}^H\widetilde{\mathbf{H}}_{\mathrm{E}}\mathbf{x}_k/C_k(\mathbf{x},\boldsymbol{\theta}))\ln 2}. \tag{20}$$

$\nabla_{\boldsymbol{\theta}}\mathrm{M1}k(\mathbf{x},\boldsymbol{\theta})$ and $\nabla_{\boldsymbol{\theta}}\mathrm{M2}k(\mathbf{x},\boldsymbol{\theta})$ are given by (21) and (22), as shown at the bottom of the next page.

After **Algorithm 1** converges, we update ξ and ω, and we can see that ω is increased. In **Algorithm 2**, the PDDAGP method for finding the stationary solution of $(\mathcal{P}2)$ is described.

Algorithm 2 PDDAGP Algorithm

1: **Input:** $\mathbf{x}^0, \boldsymbol{\theta}^0, \varsigma^0, \alpha^0, \tau^0, \xi, \omega > 0, \eta < 1$
2: **repeat**
3: Solve problem $(\mathcal{P}2)$ utilizing **Algorithm 1**;
4: $\mathbf{x}^* = \mathbf{x}^n, \boldsymbol{\theta}^* = \boldsymbol{\theta}^n, \varsigma^* = \varsigma^n$;
5: $\xi \leftarrow \xi + \omega h(\mathbf{x}^*, \boldsymbol{\theta}^*, P_A^{\max}, \varsigma^*)$;
6: $\omega \leftarrow \omega/\eta$;
7: **until** *convergence*;
8: **Output:** $\mathbf{x}^*, \boldsymbol{\theta}^*$

IV. FRACTIONAL PROGRAMMING SOLUTION WITH QOS CONSTRAINTS

Subject to the power constraints at the BS and the active RIS and QoS constraints, the original problem of maximizing the sum rate can be formulated as follows:

$$\widetilde{\mathcal{P}}_0 : \max_{x,\Phi} R_{sum}(x,\Phi) = \sum_{k=1}^{K}\{\mathrm{R}_k^{\mathrm{B}}(\mathbf{x},\boldsymbol{\theta}) - \mathrm{R}_k^{\mathrm{E}}(\mathbf{x},\boldsymbol{\theta})\}$$

Algorithm 3 Proposed Joint Transmit Beamforming and Reflect Precoding Scheme With QoS Constraints

Require: Channels $\mathbf{H}_{\mathrm{BI}}$, $\mathbf{H}_{\mathrm{BU},k}$, and $\mathbf{H}_{\mathrm{IU},k}$, $\forall k \in \{1,\cdots,K\}$.
Ensure: Optimized *basestation*(BS) beamforming vector x, optimized RIS precoding matrix of active RIS $\boldsymbol{\Phi}$, and optimized secure-rate $\mathrm{R}_k^{\mathrm{sec}}$.
1: Randomly initialize x and $\boldsymbol{\Phi}$;
2: **while** no convergence of $\mathrm{R}_k^{\mathrm{sec}}$ **do**
3: Update $\boldsymbol{\rho}$ by (29);
4: Update $\boldsymbol{\varpi}$ by (30);
5: Update w by solving (31);
6: Update $\boldsymbol{\Phi}$ by solving (33);
7: Update $\mathrm{R}_k^{\mathrm{sec}}$ by (6);
8: **end while**
9: **return** Optimized $\mathbf{x}$, $\boldsymbol{\Phi}$, **and** $\mathrm{R}_k^{\mathrm{sec}}$.

$$\begin{aligned} s.t.\ \ & C_1: \|x\|^2 \le P_{\mathrm{BS}}^{\max}, \\ & C_2: \sum_{k=1}^{K}\left\|\Phi^H\mathbf{H}_{\mathrm{BI}}\mathbf{x}_k\right\|^2 + \left\|\Phi^H\right\|_F^2\sigma_v^2 \le P_{\mathrm{A}}^{\max}, \\ & C_3: \mathrm{R}_k^{\mathrm{B}}(\mathbf{x},\boldsymbol{\theta}) \ge \eta_k, \\ & C_4: \mathrm{R}_k^{\mathrm{E}}(\mathbf{x},\boldsymbol{\theta}) \le \eta_{e,k} \end{aligned} \tag{23}$$

There are $2K$ non-convex sum-of-logarithms and fractions need to be dealed with. First we cope with the former K ones with FP technique as the following Lemma.

Lemma 1 (Relaxed Problem For Secure Sum-Rate Maximization With Qos Constraints:) With adding the slack variables $\boldsymbol{\rho} := [\rho_1,\cdots,\rho_K] \in \mathbb{R}_+^K$ and $\boldsymbol{\varpi} := [\varpi_1,\cdots,\varpi_K] \in \mathbb{C}^K$, the high nonconvex primal problem $\widetilde{\mathcal{P}}_0$ in (23) can be relaxed but with the same local optimal solutions as follows

$$\begin{aligned} \tilde{\mathcal{P}}_1 : & \max_{x,\Phi^H,\boldsymbol{\rho},\boldsymbol{\varpi}} R'_{sum}(x,\Phi^H,\boldsymbol{\rho},\boldsymbol{\varpi}) = \sum_{k=1}^{K}\ln(1+\rho_k) \\ & - \sum_{k=1}^{K}\rho_k + \sum_{k=1}^{K} g(x,\Phi^H,\rho_k,\varpi_k) - \mathrm{R}_k^{\mathrm{E}}(\mathbf{x},\boldsymbol{\theta}), \\ s.t. \quad & C_1: \|x\|^2 \le P_{\mathrm{BS}}^{\max}, \\ & C_2: \sum_{k=1}^{K}\left\|\Phi^H\mathbf{H}_{\mathrm{BI}}\mathbf{x}_k\right\|^2 + \left\|\Phi^H\right\|_F^2\sigma_v^2 \le P_{\mathrm{A}}^{\max}, \\ & C_3: \mathrm{R}_k^{\mathrm{B}}(\mathbf{x},\boldsymbol{\theta}) \ge \eta_k, \\ & C_4: \mathrm{R}_k^{\mathrm{E}}(\mathbf{x},\boldsymbol{\theta}) \le \eta_{e,k} \end{aligned} \tag{24}$$

where function $g(x,\Phi^H,\rho_k,\varpi_k)$ is defined as

$$g(x,\Phi^H,\rho_k,\varpi_k) = 2\sqrt{(1+\rho_k)}\Re\left\{\varpi_k^*\widetilde{\mathbf{H}}_{\mathrm{B},k}\mathbf{x}_k\right\} - |\varpi_k|^2\left(\sum_{j=1}^{K}\left|\widetilde{\mathbf{H}}_{\mathrm{B},k}\mathbf{x}_j\right|^2 + \left\|\mathbf{H}_{\mathrm{IU},k}\Phi\right\|^2\sigma_v^2 + \sigma^2\right). \tag{25}$$

Proof: The original proof based on Lagrange dual theory can be found in [16]. ■

Then we cope with the other K non-convex sum-of-logarithms and fractions in $\mathrm{R}_k^{\mathrm{E}}(\mathbf{x},\boldsymbol{\theta})$ based on difference of convex (DC) framework [28], and obtain

$$\begin{aligned}\widetilde{\mathcal{P}}_2:\ &\max_{x,\Phi^H,\boldsymbol{\rho},\boldsymbol{\varpi}} R'_{sum}(x,\Phi^H,\boldsymbol{\rho},\boldsymbol{\varpi})=\sum_{k=1}^{K}\ln(1+\rho_k)-\sum_{k=1}^{K}\rho_k\\&+\sum_{k=1}^{K}g(x,\Phi^H,\rho_k,\varpi_k)-(\nabla_{\mathbf{x}_k}\mathrm{A2}(\mathbf{x},\boldsymbol{\theta}))^H(x-x^n)\\&-(\nabla_{\boldsymbol{\theta}}\mathrm{M2}k(\mathbf{x},\boldsymbol{\theta}))^H(\boldsymbol{\theta}-\boldsymbol{\theta}^n),\\ s.t.\quad &C_1:\|x\|^2\le P_{\mathrm{BS}}^{\max},\\&C_2:\sum_{k=1}^{K}\left\|\Phi^H\mathbf{H}_{\mathrm{BI}}\mathbf{x}_k\right\|^2+\left\|\Phi^H\right\|_F^2\sigma_v^2\le P_{\mathrm{A}}^{\max},\\&C_3:\mathrm{R}_k^{\mathrm{B}}(\mathbf{x},\boldsymbol{\theta})\ge\eta_k,\\&C_4:\mathrm{R}_k^{\mathrm{E}}(\mathbf{x},\boldsymbol{\theta})\le\eta_{e,k}\end{aligned}\tag{26}$$

Now we need to deal with nonconvex QoS constraints C_3 and C_4 via the following successive convex approximation (SCA) lemmas.

Lemma 2: if

$$\begin{aligned}&\tilde{C}_3:2\mathrm{Re}\{\widetilde{\mathbf{H}}_{\mathrm{B},k}\mathbf{x}_k\}-\|\widetilde{\mathbf{H}}_{\mathrm{B},k}\mathbf{x}_k^n\|^2\ge\\&(\|\widetilde{\mathbf{H}}_{\mathrm{B},k}\|^2P_{\mathrm{BS}}^{\max}+\left\|\mathbf{H}_{\mathrm{IU},k}\Phi\right\|^2\sigma_v^2+\sigma)(1-2^{-\eta_k}).\end{aligned}\tag{27}$$

is satisfied, we have $C_3:\mathrm{R}_k^{\mathrm{B}}(\mathbf{x},\boldsymbol{\theta})\ge\eta_k$.

Proof: Please see Appendix A. ■

Lemma 3: if $C_4:\mathrm{R}_k^{\mathrm{E}}(\mathbf{x},\boldsymbol{\theta})\le\eta_{e,k}$ is satisfied, we have

$$\begin{aligned}\tilde{C}_4:\|\widetilde{\mathbf{H}}_{\mathrm{E}}\mathbf{x}_k\|^2\le&(\sum_{i\neq k}\{2\mathrm{Re}\{\widetilde{\mathbf{H}}_{\mathrm{E}}\mathbf{x}_i\}-\|\widetilde{\mathbf{H}}_{\mathrm{E}}\mathbf{x}_i^n\|^2\}\\&+\|\mathbf{H}_{\mathrm{IE}}\Phi\|^2\sigma_v^2+\sigma_e)(2^{\eta_{e,k}}-1).\end{aligned}\tag{28}$$

Proof: Please see Appendix B. ■

Based on Lemma 2 and 3, thus, we have

$$\begin{aligned}\widetilde{\mathcal{P}}_3:\ &\max_{x}\ \Re\left\{2b^Hx\right\}-x^HAw-(\nabla_{\mathbf{x}_k}\mathrm{A2}(\mathbf{x},\boldsymbol{\theta}))^H\\&(x-x^n),\\ s.t.\quad &C_1:\|x\|^2\le P_{\mathrm{BS}}^{\max},\\&C_2:x^H\Xi w\le P_{\mathrm{m}}^{\max},\\&\tilde{C}_3:(27),\\&\tilde{C}_4:(28).\end{aligned}$$

Although $\widetilde{\mathcal{P}}_3$ is nonconvex for the whole optimization problem, if fixing three of x, Φ^H, $\boldsymbol{\rho}$, $\boldsymbol{\varpi}$, the original problem relaxed to be a convex subproblem, and we can optimize x, Φ^H, $\boldsymbol{\rho}$, $\boldsymbol{\varpi}$ in an alternative way as follows.

A. UPDATING ρ

By setting $\frac{\partial R'_{\mathrm{sum}}}{\partial\rho_k}=0$, we obtain

$$\rho_k^{opt}=\frac{\xi_k^2+\xi_k\sqrt{\xi_k^2+4}}{2},\quad\forall k\in\{1,\cdots,K\},\tag{29}$$

where $\xi_k=\Re\left\{\varpi_k^*\widetilde{\mathbf{H}}_{\mathrm{B},k}\mathbf{x}_k\right\}$.

B. UPDATING ϖ

By solving $\frac{\partial R'_{\mathrm{sum}}}{\partial\varpi_k}=0$, we have

$$\varpi_k^{\mathrm{opt}}=\frac{\sqrt{(1+\rho_k)}\widetilde{\mathbf{H}}_{\mathrm{B},k}\mathbf{x}_k}{\sum_{j=1}^{K}\left|\widetilde{\mathbf{H}}_{\mathrm{B},k}\mathbf{x}_j\right|^2+\left\|\mathbf{H}_{\mathrm{IU},k}\Phi\right\|^2\sigma_v^2+\sigma^2},\quad\forall k\in\{1,\cdots,K\}.$$

C. FIXING OTHER VARIABLES, OPTIMIZING X

To simplify the notations, we first introduce the following definitions:

$$b_k^H=\sqrt{(1+\rho_k)}\varpi_k^*\widetilde{\mathbf{H}}_{\mathrm{B},k},\quad b=\left[b_1^T,b_2^T,\cdots,b_N^T\right]^T,\tag{30a}$$

$$\nabla_{\mathbf{x}_k}\mathrm{A1}(\mathbf{x},\boldsymbol{\theta})=\frac{\widetilde{\mathbf{H}}_{\mathrm{B},k}^H\widetilde{\mathbf{H}}_{\mathrm{B},k}\mathbf{x}_k/B_k(\mathbf{x},\boldsymbol{\theta})}{(1+\mathbf{x}_k^H\widetilde{\mathbf{H}}_{\mathrm{B},k}^H\widetilde{\mathbf{H}}_{\mathrm{B},k}\mathbf{x}_k/B_k(\mathbf{x},\boldsymbol{\theta}))\ln 2}-\sum_{m\in\mathcal{K},m\neq k}\frac{\widetilde{\mathbf{H}}_{\mathrm{B},m}^H\widetilde{\mathbf{H}}_{\mathrm{B},m}\mathbf{x}_k(\mathbf{x}_m^H\widetilde{\mathbf{H}}_{\mathrm{B},m}^H\widetilde{\mathbf{H}}_{\mathrm{B},m}\mathbf{x}_m)/(B_m(\mathbf{x},\boldsymbol{\theta}))^2}{(1+\mathbf{x}_m^H\widetilde{\mathbf{H}}_{\mathrm{B},m}^H\widetilde{\mathbf{H}}_{\mathrm{B},m}\mathbf{x}_m/B_m(\mathbf{x},\boldsymbol{\theta}))\ln 2}.\tag{15}$$

$$\nabla_{\mathbf{x}_k}\mathrm{A2}(\mathbf{x},\boldsymbol{\theta})=\frac{\widetilde{\mathbf{H}}_{\mathrm{E}}^H\widetilde{\mathbf{H}}_{\mathrm{E}}\mathbf{x}_k/C_k(\mathbf{x},\boldsymbol{\theta})}{(1+\mathbf{x}_k^H\widetilde{\mathbf{H}}_{\mathrm{E}}^H\widetilde{\mathbf{H}}_{\mathrm{E}}\mathbf{x}_k/C_k(\mathbf{x},\boldsymbol{\theta}))\ln 2}-\sum_{m\in\mathcal{K},m\neq k}\frac{\widetilde{\mathbf{H}}_{\mathrm{E}}^H\widetilde{\mathbf{H}}_{\mathrm{E}}\mathbf{x}_k(\mathbf{x}_m^H\widetilde{\mathbf{H}}_{\mathrm{E}}^H\widetilde{\mathbf{H}}_{\mathrm{E}}\mathbf{x}_m)/(C_m(\mathbf{x},\boldsymbol{\theta}))^2}{(1+\mathbf{x}_m^H\widetilde{\mathbf{H}}_{\mathrm{E}}^H\widetilde{\mathbf{H}}_{\mathrm{E}}\mathbf{x}_m/C_m(\mathbf{x},\boldsymbol{\theta}))\ln 2}.\tag{16}$$

$$\begin{aligned}\nabla_{\boldsymbol{\theta}}\mathrm{M1}k(\mathbf{x},\boldsymbol{\theta})=&\frac{\mathrm{vec_d}(\mathbf{H}_{\mathrm{IU},k}^H\widetilde{\mathbf{H}}_{\mathrm{B},k}\mathbf{x}_k\mathbf{x}_k^H\mathbf{H}_{\mathrm{BI}}^H)}{B_k(\mathbf{x},\boldsymbol{\theta})}\\&-\frac{\sum_{i\in\mathcal{K},i\neq k}\mathrm{vec_d}(\mathbf{H}_{\mathrm{IU},k}^H\widetilde{\mathbf{H}}_{\mathrm{B},k}\mathbf{x}_i\mathbf{x}_i^H\mathbf{H}_{\mathrm{BI}}^H)\mathbf{x}_k^H\widetilde{\mathbf{H}}_{\mathrm{B},k}^H\widetilde{\mathbf{H}}_{\mathrm{B},k}\mathbf{x}_k+\mathrm{vec_d}(\mathbf{H}_{\mathrm{IU},k}^H\mathbf{H}_{\mathrm{IU},k}\Phi^H)\sigma_v^2\mathbf{x}_k^H\widetilde{\mathbf{H}}_{\mathrm{B},k}^H\widetilde{\mathbf{H}}_{\mathrm{B},k}\mathbf{x}_k}{B_k(\mathbf{x},\boldsymbol{\theta})^2}.\end{aligned}\tag{21}$$

$$\nabla_{\boldsymbol{\theta}}\mathrm{M2}k(\mathbf{x},\boldsymbol{\theta})=\frac{\mathrm{vec_d}(\mathbf{H}_{\mathrm{IE}}^H\widetilde{\mathbf{H}}_{\mathrm{E}}\mathbf{x}_k\mathbf{x}_k^H\mathbf{H}_{\mathrm{BI}}^H)}{C_k(\mathbf{x},\boldsymbol{\theta})}-\frac{\sum_{i\in\mathcal{K},i\neq k}\mathrm{vec_d}(\mathbf{H}_{\mathrm{IE}}^H\widetilde{\mathbf{H}}_{\mathrm{E}}\mathbf{x}_i\mathbf{x}_i^H\mathbf{H}_{\mathrm{BI}}^H)\mathbf{x}_k^H\widetilde{\mathbf{H}}_{\mathrm{E}}^H\widetilde{\mathbf{H}}_{\mathrm{E}}\mathbf{x}_k+\mathrm{vec_d}(\mathbf{H}_{\mathrm{IE}}^H\mathbf{H}_{\mathrm{IE}}\Phi^H)\sigma_v^2\mathbf{x}_k^H\widetilde{\mathbf{H}}_{\mathrm{E}}^H\widetilde{\mathbf{H}}_{\mathrm{E}}\mathbf{x}_k}{C_k(\mathbf{x},\boldsymbol{\theta})^2}.\tag{22}$$

$$A = I_K \otimes \sum_{k=1}^{K} |\varpi_k|^2 \widetilde{\mathbf{H}}_{\mathrm{B},k}^H \widetilde{\mathbf{H}}_{\mathrm{B},k},$$

$$\Xi = I_K \otimes \left(\mathbf{H}_{\mathrm{BI}}{}^H \Phi^H \Phi^H \mathbf{H}_{\mathrm{BI}} \right), \tag{30b}$$

$$P_{\mathrm{m}}^{\max} = P_{\mathrm{A}}^{\max} - \|\Phi\|_F^2 \sigma_v^2. \tag{30c}$$

Then, for fixed RIS precoding matrix Φ and auxiliary variables $\boldsymbol{\rho}$ and $\boldsymbol{\varpi}$, problem $\widetilde{\mathcal{P}}_2$ in (26) can be reformulated as follows

$$\begin{aligned} \widetilde{\mathcal{P}}_4: \ & \max_{x} \ \Re\left\{2b^H x\right\} - x^H A w \quad - (\nabla_{\mathbf{x}_k} \mathrm{A2}(\mathbf{x}, \boldsymbol{\theta}))^H \\ & \times (x - x^n), \\ s.t. \ \ & C_1: \|x\|^2 \le P_{\mathrm{BS}}^{\max}, \\ & C_2: x^H \Xi w \le P_{\mathrm{m}}^{\max}, \\ & C_3: \mathrm{R}_k^{\mathbb{B}}(\mathbf{x}, \boldsymbol{\theta}) \ge \eta_k, \\ & C_4: \mathrm{R}_k^{\mathbb{E}}(\mathbf{x}, \boldsymbol{\theta}) \le \eta_{e,k}. \end{aligned} \tag{31}$$

which belong to traditional QCQP problems, and can be efficiently solved using mathematical optimization tools such as CVX.

D. FIXING OTHER VARIABLES, OPTIMIZING θ

For the simplicity of optimizing $\boldsymbol{\theta}$, the combining channel $\widetilde{\mathbf{H}}_{\mathrm{B},k}$ is equivalent to the following form:

$$\begin{aligned} \widetilde{\mathbf{H}}_{\mathrm{B},k} &= \mathbf{H}_{\mathrm{BU},k} + \mathbf{H}_{\mathrm{IU},k} \Phi^H \mathbf{H}_{\mathrm{BI}} \\ &= \mathbf{H}_{\mathrm{BU},k} + \boldsymbol{\theta}^{\mathrm{H}} \mathrm{diag}\left(\mathbf{H}_{\mathrm{IU},k}\right) \mathbf{H}_{\mathrm{BI}}. \end{aligned} \tag{32}$$

Utilizing (32), the problem $\widetilde{\mathcal{P}}_2$ in (26) with respect to $\boldsymbol{\theta}$ can be reformulated as follows:

$$\begin{aligned} \tilde{\mathcal{P}}_5: \ & \max_{\boldsymbol{\theta}} \ \Re\left\{2\boldsymbol{\theta}^H \boldsymbol{\upsilon}\right\} - \boldsymbol{\theta}^H \boldsymbol{\Omega} \boldsymbol{\theta} - (\nabla_{\boldsymbol{\theta}} \mathrm{M2}k(\mathbf{x}, \boldsymbol{\theta}))^H \\ & \times (\boldsymbol{\theta} - \boldsymbol{\theta}^n), \\ s.t. \ \ & C_2: \boldsymbol{\theta}^H \boldsymbol{\Pi} \boldsymbol{\theta} \le P_{\mathrm{A}}^{\max}, \\ & C_3: \mathrm{R}_k^{\mathbb{B}}(\mathbf{x}, \boldsymbol{\theta}) \ge \eta_k, \\ & C_4: \mathrm{R}_k^{\mathbb{E}}(\mathbf{x}, \boldsymbol{\theta}) \le \eta_{e,k}. \end{aligned} \tag{33}$$

wherein

$$\boldsymbol{\upsilon} = \sum_{k=1}^{K} \sqrt{(1+\rho_k)} \mathrm{diag}\left(\varpi_k^* \mathbf{H}_{\mathrm{IU},k}\right) \mathbf{H}_{\mathrm{BI}} \mathbf{x}_k - \sum_{k=1}^{K} |\varpi_k|^2 \mathrm{diag}\left(\mathbf{H}_{\mathrm{IU},k}\right) \mathbf{H}_{\mathrm{BI}} \sum_{j=1}^{K} \mathbf{x}_j x_j^H \mathbf{H}_{\mathrm{BU},k}^H, \tag{34a}$$

$$\boldsymbol{\Omega} = \sum_{k=1}^{K} |\varpi_k|^2 \mathrm{diag}\left(\mathbf{H}_{\mathrm{IU},k}\right) \mathrm{diag}\left(\mathbf{H}_{\mathrm{IU},k}{}^H\right) \sigma_v^2 + \sum_{k=1}^{K} |\varpi_k|^2 \sum_{j=1}^{K} \mathrm{diag}\left(\mathbf{H}_{\mathrm{IU},k}\right) \mathbf{H}_{\mathrm{BI}} \mathbf{x}_j x_j^H \mathbf{H}_{\mathrm{BI}}{}^H \mathrm{diag}(\mathbf{H}_{\mathrm{BI}} \mathbf{H}_{\mathrm{IU},k}^H), \tag{34b}$$

$$\Pi = \sum_{k=1}^{K} \mathrm{diag}\left(\mathbf{H}_{\mathrm{BI}} \mathbf{H}_{\mathrm{IU},k}^H\right) \left(\mathrm{diag}\left(\mathbf{H}_{\mathrm{BI}} \mathbf{H}_{\mathrm{IU},k}^H\right)\right)^H + \sigma_v^2 I_N. \tag{34c}$$

Although QoS constraints C_3 and C_4 can be reformulated into more conservative but convex constraints with respect to $\boldsymbol{\theta}$, it will result in high computational complexity of the whole algorithm. Therefore, we are shifting towards a low-complexity operation, focusing on optimizing the $\boldsymbol{x}$ sub-problem to meet QoS constraints, while optimizing $\boldsymbol{\theta}$ to enhance overall security rate. Omitting the satisfactory of C_3 and C_4 in updating θ, we have

$$\begin{aligned} \tilde{\mathcal{P}}_6: \ & \max_{\boldsymbol{\theta}} \ \Re\left\{2\boldsymbol{\theta}^H \boldsymbol{\upsilon}\right\} - \boldsymbol{\theta}^H \boldsymbol{\Omega} \boldsymbol{\theta} - (\nabla_{\boldsymbol{\theta}} \mathrm{M2}k(\mathbf{x}, \boldsymbol{\theta}))^H (\boldsymbol{\theta} - \boldsymbol{\theta}^n), \\ s.t. \ \ & C_2: \boldsymbol{\theta}^H \boldsymbol{\Pi} \boldsymbol{\theta} \le P_{\mathrm{A}}^{\max}, \end{aligned} \tag{35}$$

Based on Lagrange dual theory, $\boldsymbol{\theta}^{opt}$ can be obtained by finding the optimal Lagrange multiplier and is listed by

$$\boldsymbol{\theta}^{opt} = (\boldsymbol{\Omega} + \mu \boldsymbol{\Pi})^{-1} \boldsymbol{\upsilon}, \tag{36}$$

where μ denotes the Lagrange multiplier, which follows the classcal KKT conditions and can be efficiently calculated via Newton method.

In summary, **Algorithm 3** focuses on tacking algorithmic challenges of the sum-rate maximization problem $\widetilde{\mathcal{P}}_0$ in (23), which aims to address the most basic issue, i.e., the joint design the BS beamforming and the active RIS precoding. Since the considered channels G, h_k, and f_k are arbitrary, regardless of the specific CSI, the proposed algorithm works as a feasible solution to improve the performance gain of active RISs in communication systems. Besides, since the proposed algorithm decouples different variables to be optimized, this algorithm has a good expansibility, which can serve as a framework for the possible algorithmic improvements in future works, such as addressing non-ideal CSI and reducing computational complexity.

E. APPROXIMATION IN DISCRETE PHASE SHIFT CASE

Denote $\mathcal{F}_{\mathrm{dps}}$ as the practical case where the low-resolution phase of θ is discrete, i.e.,

$$\mathcal{F}_{\mathrm{dps}} \triangleq \left\{ \boldsymbol{\theta} \middle| \theta_n \in \left\{ 1, e^{j\frac{2\pi}{L}}, \cdots, e^{j\frac{2\pi(L-1)}{L}} \right\} \right\}, \tag{37a}$$

where L indicates that $\mathcal{F}_{\mathrm{dps}}$ contains L discrete phase shifts. When $\mathcal{F}_{\mathrm{dps}}$, the common solution to address the non-convex constraint of discrete space is approximation projection [21]. Specifically, we can first relax $\mathcal{F}_{\mathrm{dps}}$ to continuous phase shift case, and obtain the optimal solution $\boldsymbol{\theta}^{opt}$ by solving (35). Then, following the proximity principle, we can simply project the solved $\boldsymbol{\theta}^{opt}$ to the elements in $\mathcal{F}_{\mathrm{dps}}$ by a approximation projection, written as

$$\angle \boldsymbol{\theta}^{sub} = \underset{\boldsymbol{\phi} \in \mathcal{F}_{dps}}{\mathrm{argmin}} \left| \angle \boldsymbol{\theta}^{\mathrm{opt}} - \angle \boldsymbol{\phi} \right|, \tag{38a}$$

$$\boldsymbol{\Theta}^{\mathrm{opt}} = diag(exp(j\mathrm{arg}(\boldsymbol{\theta}^{\mathrm{sub}})), \tag{38b}$$

$$\boldsymbol{a}^{\mathrm{opt}} = diag(exp(-jarg(\boldsymbol{\theta}^{\mathrm{sub}}))\boldsymbol{\theta}^{\mathrm{sub}}, \tag{38c}$$

where $\boldsymbol{\theta}^{sub}$ denotes the approximated sub-optimal solution to the phase shift $\boldsymbol{\theta}$. Thus, we can finally obtain the sub-optimal solution $\boldsymbol{\Theta}^{sub} \in \mathcal{F}_{\mathrm{dps}}$ to the subproblem (35).

V. FRAMEWORK SUPPLEMENTS

In this section, we first provide practical implications of proposed methods in Subsection V-A. Then, we analyze the convergency and computational complexity of the proposed algorithms in Subsection V-B.

A. PRACTICAL IMPLICATIONS AND FEASIBILITY OF IMPLEMENTATION

From theoretical analysis to optimization models and hardware implementation, the deployment and application prospects of passive RIS have been studied and confirmed by numerous researchers. Particularly in scenarios where direct paths are absent, passive RIS indeed exhibits superior performance and practical value by compensating for the challenges posed by the lack of direct links through RIS reflection. However, once direct paths exist, the application of passive RIS can trigger multiplicative fading effects, limiting its ability to enhance performance. This is where the value of active RIS becomes evident: by adding reflection-type amplifier hardware on top of passive RIS, implemented through such methods as current-inverting converters [23], asymmetric current mirrors [24], or some integrated circuits [25], active RIS systems significantly improve system performance metrics including signal-to-noise ratio (SNR), throughput, and energy efficiency.

B. CONVERGENCE AND COMPLEXITY OF THE DEVELOPED SOLUTION

1) PROOF OF CONVERGENCE

The proof approach for **Algorithm 2** is analogous to that in [18], and we summarize it as follows. Firstly, after ξ and ω are fixed, **Algorithm 1** produces a strictly ascending sequence of target values, denoted as $\bar{\mathrm{R}}^{\mathrm{sec}}_{\xi,\omega}(\mathbf{x},\boldsymbol{\theta},\varsigma)$. As the feasible domain is bounded, the monotonically increasing sequence converges asymptotically to the limit point of (9a) with a certain accuracy ϵ and $\|\xi^{k+1}-\xi^{k}\|$ is bounded. Therefore, according to the update of the Lagrange multiplier, it implies that $\sqrt{h^2(\mathbf{x},\boldsymbol{\theta},P_{\mathrm{A}}^{\max},\varsigma)}=\frac{1}{\omega}\|\xi^{k+1}-\xi^{k}\|\to 0$ as $\frac{1}{\omega}\to 0$. The key to this proof lies in demonstrating that the target sequence $\bar{\mathrm{R}}^{\mathrm{sec}}_{\xi,\omega}(\mathbf{x},\boldsymbol{\theta},\varsigma)$ generated by **Algorithm 1** is strictly increasing and bounded. By ensuring the boundedness of the sequence, we can verify the convergence of the dual update and ultimately obtain the optimal solution.

2) COMPLEXITY ANALYSIS

Clearly, the analysis of the complexity of **Algorithm 2** is significantly influenced by the complexity of **Algorithm 1**. Therefore, we first examine the complexity of $\nabla_{\mathbf{x}}\bar{\mathrm{R}}^{\mathrm{sec}}_{\xi,\omega}(\mathbf{x},\boldsymbol{\theta},\varsigma)$ in **Algorithm 1**. The complexity of $\nabla_{\mathbf{x}}\bar{\mathrm{R}}^{\mathrm{sec}}_{\xi,\omega}(\mathbf{x},\boldsymbol{\theta},\varsigma)$ is mainly related to $\nabla_{\mathbf{x}_k}\mathrm{R}^{\mathrm{sec}}(\mathbf{x},\boldsymbol{\theta})$. The computational complexity of $\mathbf{H}_{\mathrm{B},k}$ and $\mathbf{H}_{\mathrm{E}}$ is both $\mathcal{O}(NM)$. Therefore, according to (14), (15) and (16), it can be concluded that the complexity of $\nabla_{\mathbf{x}_k}\mathrm{R}^{\mathrm{sec}}(\mathbf{x},\boldsymbol{\theta})$, is $\mathcal{O}(K(KM+N))$. From (14), we can see that the complexity of computing $\nabla_{\mathbf{x}_k}\bar{\mathrm{R}}^{\mathrm{sec}}_{\xi,\omega}(\mathbf{x},\boldsymbol{\theta},\varsigma)$ is $\mathcal{O}(K(KM+N))$, and the complexity of computing $\nabla_{\mathbf{x}}\bar{\mathrm{R}}^{\mathrm{sec}}_{\xi,\omega}(\mathbf{x},\boldsymbol{\theta},\varsigma)$ is $\mathcal{O}(K^2(KM+N))$. Ignoring the negligible terms α^n and $\Pi_{\mathcal{X}}(\cdot)$, the per-iteration complexity of step 5 in **Algorithm 1** is $\mathcal{O}(KNM+K^2(KM+N))$.

Next, we calculate the complexity of $\nabla_{\boldsymbol{\theta}}\bar{\mathrm{R}}^{\mathrm{sec}}_{\xi,\omega}(\mathbf{x},\boldsymbol{\theta},\varsigma)$. From (18), (19) and (20), it can be concluded that the complexity of $\nabla_{\boldsymbol{\theta}}\mathrm{R}^{\mathrm{sec}}(\mathbf{x},\boldsymbol{\theta})$ is $\mathcal{O}(K^2NM)$. This makes the complexity of $\nabla_{\boldsymbol{\theta}}\bar{\mathrm{R}}^{\mathrm{sec}}_{\xi,\omega}(\mathbf{x},\boldsymbol{\theta},\varsigma)$ to be $\mathcal{O}(K^2NM)$. The complexity associated with the values of τ^n and $\Pi_{\Theta}(\cdot)$ is relatively small, so it can be ignored. Therefore, step 6 in **Algorithm 1** has the same complexity as $\nabla_{\boldsymbol{\theta}}\bar{\mathrm{R}}^{\mathrm{sec}}_{\xi,\omega}(\mathbf{x},\boldsymbol{\theta},\varsigma)$. Compared with $\mathbf{x}^n$(step 5) and $\boldsymbol{\theta}^n$(step 6), the complexity of step 7 can be ignored. According to the above discussion, the total complexity per-iteration for **Algorithm 1** can be represented as $\mathcal{O}(K^2NM+K^2(KM+N))$. This means that the overall complexity of **Algorithm 2** per-iteration is

$$\mathcal{O}(K^2NM+K^2(KM+N)). \tag{39}$$

However, in a practical active RIS-assisted multiuser MISO system, $N \gg max\{K,M\}$. The overall per-iteration complexity of **Algorithm 2** can be approximately $\mathcal{O}(K^2NM)$, which is linearly related to the number of RIS tiles.

The computational complexity of **Algorithm 3** is mainly related to alternatively optimizing four variables $\boldsymbol{\rho}$, $\boldsymbol{\varpi}$, w, and $\boldsymbol{\Psi}$ via (29), (30), (31), and (33), respectively. Specifically, the computational complexity of computing $\boldsymbol{\rho}$ and $\boldsymbol{\varpi}$ are $\mathcal{O}(KM)$ and $\mathcal{O}\left(K^2M+KN\right)$, respectively. Both w and $\boldsymbol{\Psi}$ need to solve a standard convex QCQP problem. Thus, the computational complexity of updating w and $\boldsymbol{\Psi}$ are $\mathcal{O}\left(\log_2\left(1/\varepsilon\right)\sqrt{MK+2}\,(1+MK)\,M^3K^3\right)$ and $\mathcal{O}\left(\log_2\left(1/\varepsilon\right)\sqrt{N+1}\,(1+2N)\,N^3\right)$, respectively. As such, the whole computational complexity of **Algorithm 3** is upper bounded by $\mathcal{O}\left(\log_2\left(1/\varepsilon\right)I_o\left(M^{4.5}K^{4.5}+N^{4.5}\right)\right)$, wherein ε and I_o represent the given accuracy tolerance the number of iterations required by **Algorithm 3** for convergence, respectively.

VI. SIMULATION RESULTS

In this section, the performance of the proposed PDDAPG method is evaluated. The BS and RIS are positioned at coordinates (0 m, -60 m) and (300 m, 10 m), respectively. K Bobs are randomly distributed within a circular area centered at (300 m, 0 m) with a radius of 50 m. Eve is randomly located within a circular region centered at (400 m, 0 m) with a radius of 5 m. Similar to [10], the large-scale path loss is $PL = 10^{-3.73}(d_{link})^{-a}$, where a represents the path-loss exponent and d_{link} denotes the distance between two devices. The channels are comprised of both large-scale fading and small-scale fading, with the latter following a Rician distribution. We set a_{BE}, a_{BI}, a_{IU}, a_{IE}, and a_{BU} to represent the path-loss exponents of BS-Eve link, BS-RIS link, RIS-Bob link, RIS-Eve link, and BS-Bob link respectively. By carefully selecting the position of the RIS, the links related to the RIS may experience path loss close to free space [19]. Therefore, we set the path loss exponent of the links related to the RIS to $a_{\mathrm{BI}}=a_{\mathrm{IU}}=a_{\mathrm{IE}}=2.2$. Unless specified otherwise, in this section we set $a_{\mathrm{BU}}=3.8$, $a_{\mathrm{BE}}=3.5$, $M=4$, $N=64$,

$K = 2$, $\zeta = 0.5$, $P^{\max} = 20$ dBm, $P_{\mathrm{A}}^{\max} = 0.01 \times P^{\max}$, $P_{\mathrm{BS}}^{\max} = 0.99 \times P^{\max}$. The maximum achievable amplitude is $\beta_{n,\max} = 100, \forall n \in \mathcal{N}$. In **Algorithm 2**, we start with $\omega = 0.001$ and increase it to $\omega \leftarrow \omega/\eta$ where $\eta = 0.8$. Furthermore, we assume that $\sigma_e^2 = -100$ dBW, $\sigma_v^2 = \sigma^2 = B\mathcal{N}_0$, the system bandwidth is $B = 20$ MHz and the noise power spectral density $\mathcal{N}_0 = -174$ dBm/Hz.

In this paper, the secure spectrum efficiency is defined as the achievable sum rate in (23), and the secure energy efficiency is defined as the ratio between the achievable sum rate and the total power consumption, i.e

$$Secure\ EE = \frac{R_{sum}(x, \Phi)}{P} \tag{40}$$

with $P = \xi \sum_{k=1}^{K} \|x\|^2 + \varphi(\sum_{k=1}^{K} \left\|\Phi^H \mathbf{H}_{\mathrm{BI}} \mathbf{x}_k\right\|^2 + \left\|\Phi^H\right\|_F^2 \sigma_v^2) + KW_u + W_{BS} + NW_{PS} + LW_{PA}$, where ξ and ϖ denote the energy transmission parameters. W_u, W_{BS}, W_{PS}, and W_{PA} represent the consumed power at users, BS, phase shift circuit and power amplifier of RIS, respectively.

Next, we present the simulation results to evaluate the performance of the proposed PDDAPG method in an active RIS-assisted multiuser MISO system, and compare the proposed method with the following existing methods:

- The algorithm based on DFAO in [10] is extended to the active RIS-assisted multiuser MISO system (denoted as FP (active RIS) [10]). Specifically, we handle the $\sum_{k\in\mathcal{K}} \mathrm{R}_k^{\mathrm{E}}(\mathbf{x}, \boldsymbol{\theta})$ part of (7a) using the first-order Taylor expansion and define $\mathrm{A2}(\mathbf{x}, \boldsymbol{\theta}) = \sum_{k\in\mathcal{K}} \mathrm{A2}k(\mathbf{x}, \boldsymbol{\theta}) = \sum_{k\in\mathcal{K}} \mathrm{R}_k^{\mathrm{E}}(\mathbf{x}, \boldsymbol{\theta})$. Then, the objective function (7a) of the optimization problem $(\mathcal{P}1)$ can be converted to

$$\widehat{\mathrm{R}}^{\mathrm{sec}}(\mathbf{x}, \boldsymbol{\theta}) \triangleq \left[\sum_{k\in\mathcal{K}} \mathrm{R}_k^{\mathrm{B}}(\mathbf{x}, \boldsymbol{\theta}) - f(\mathbf{x}, \boldsymbol{\theta}, \mathbf{x}^t, \boldsymbol{\theta}^t)\right]^+, \tag{41}$$

where $f(\mathbf{x}, \boldsymbol{\theta}, \mathbf{x}^t, \boldsymbol{\theta}^t)$ represents the first-order Taylor expansion of $\mathrm{A2}(\mathbf{x}, \boldsymbol{\theta})$ expressed as

$$f(\mathbf{x}, \boldsymbol{\theta}, \mathbf{x}^t, \boldsymbol{\theta}^t) = \mathrm{A2}(\mathbf{x}^t, \boldsymbol{\theta}^t) + (\nabla_{\mathbf{x}} \mathrm{A2}(\mathbf{x}^t, \boldsymbol{\theta}^t))^H (\mathbf{x} - \mathbf{x}^t) + \sum_{k\in\mathcal{K}} (\nabla_{\boldsymbol{\theta}} \mathrm{A2}k(\mathbf{x}^t, \boldsymbol{\theta}^t))^H (\boldsymbol{\theta} - \boldsymbol{\theta}^t), \tag{42}$$

and $\mathbf{x}^t, \boldsymbol{\theta}^t$ represents the optimal values of $\mathbf{x}$ and $\boldsymbol{\theta}$ in the t-th iteration.

$$\nabla_{\mathbf{x}} \mathrm{A2}(\mathbf{x}, \boldsymbol{\theta}) = [(\nabla_{\mathbf{x}_1} \mathrm{A2}(\mathbf{x}, \boldsymbol{\theta}))^T, (\nabla_{\mathbf{x}_2} \mathrm{A2}(\mathbf{x}, \boldsymbol{\theta}))^T, \ldots, (\nabla_{\mathbf{x}_K} \mathrm{A2}(\mathbf{x}, \boldsymbol{\theta}))^T]^T.$$

$\nabla_{\mathbf{x}_k} \mathrm{A2}(\mathbf{x}, \boldsymbol{\theta})$ and $\nabla_{\boldsymbol{\theta}} \mathrm{A2}k(\mathbf{x}, \boldsymbol{\theta})$ are given by (16) and (20) respectively. We can find that the optimization variables $\mathbf{x}$ and $\boldsymbol{\theta}$ in (24) can be decoupled using the DFAO method in [10], and then the non-convex problem can be transformed into two convex subproblems using the AO algorithm for solving. It should be noted that these two subproblems are standard quadratic constraint quadratic programming (QCQP) problems and can be solved using the toolbox CVX [20].

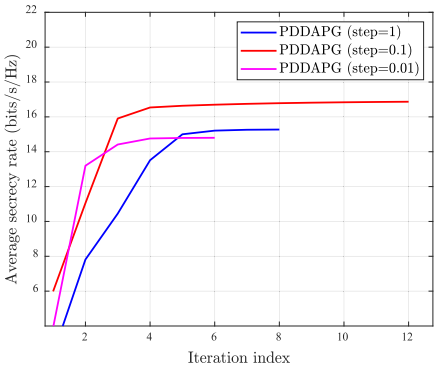

FIGURE 2. Convergence results of PDDAGP method under different step sizes.

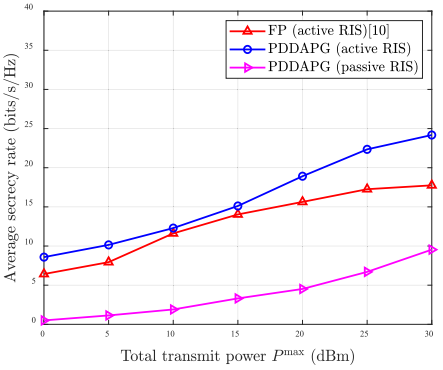

FIGURE 3. Average system sum secrecy rate versus the total power consumption $P^{\max}$.

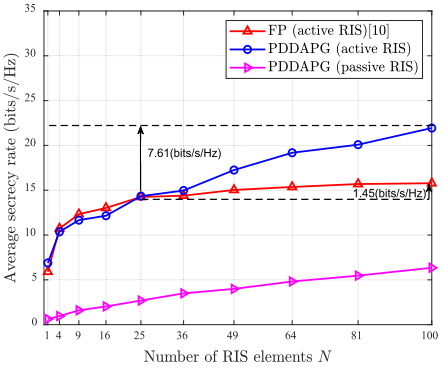

FIGURE 4. Average system sum secrecy rate versus the number of RIS elements N.

Fig. 2 shows the convergence results of **Algorithm 2** with different step size initial values ($\alpha^0 = \tau^0$). From Fig. 2, it can be clearly observed that there is little difference in the final converged secrecy rates obtained with different step sizes of initial values. The different step size initial values mainly affect the convergence speed of **Algorithm 2**. Noting that, for fixed values of ξ and ω, when $|\bar{\mathrm{R}}_{\xi,\omega}^{\mathrm{sec}}(\mathbf{x}^n, \boldsymbol{\theta}^n, \varsigma^n) - \bar{\mathrm{R}}_{\xi,\omega}^{\mathrm{sec}}(\mathbf{x}^{n-1}, \boldsymbol{\theta}^{n-1}, \varsigma^{n-1})|/\bar{\mathrm{R}}_{\xi,\omega}^{\mathrm{sec}}(\mathbf{x}^{n-1}, \boldsymbol{\theta}^{n-1}, \varsigma^{n-1})$ is less

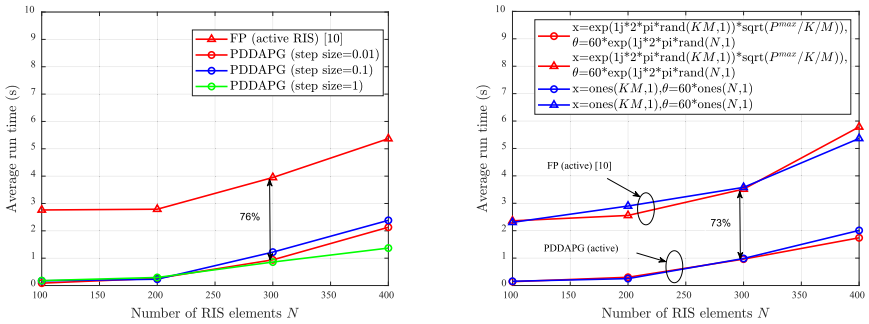

(a) (b)

FIGURE 5. Average run time comparison between the proposed PDDAPG and the AO algorithms.

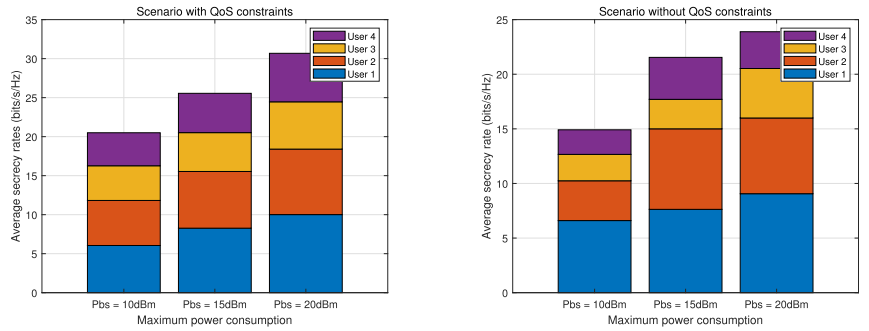

(a) (b)

FIGURE 6. The comparison of achievable secrecy rates between users with QoS constraints and those without QoS constraints.

than or equal to the tolerance value ($\epsilon = 10^{-3}$), $\bar{\mathrm{R}}^{\mathrm{sec}}_{\xi,\omega}(\mathbf{x}, \boldsymbol{\theta}, \varsigma)$ is considered to have converged. After this, we update ξ and ω. Finally, when $|\mathrm{R}^{\mathrm{sec}}(\mathbf{x}^n, \boldsymbol{\theta}^n) - \bar{\mathrm{R}}^{\mathrm{sec}}_{\xi,\omega}(\mathbf{x}^n, \boldsymbol{\theta}^n, \varsigma^n)|/\bar{\mathrm{R}}^{\mathrm{sec}}_{\xi,\omega}(\mathbf{x}^n, \boldsymbol{\theta}^n, \varsigma^n) \leq \epsilon$, **Algorithm 2** is considered to have converged. Noting that the objective of **Algorithm 1** is to maximize $\bar{\mathrm{R}}^{\mathrm{sec}}_{\xi,\omega}(\mathbf{x}, \boldsymbol{\theta}, \varsigma)$, so for fixed ξ and ω, $\bar{\mathrm{R}}^{\mathrm{sec}}_{\xi,\omega}(\mathbf{x}, \boldsymbol{\theta}, \varsigma)$ monotonically increases.

Fig. 3 shows the relationship between the average system sum secrecy rate and the total power consumption $P^{\max}$ given $N = 64$. The figure shows that as total power consumption $P^{\max}$ increases, the system sum secrecy rate under each scheme increases. Compared with DFAO algorithm, PDDAPG method achieves a higher gain of secrecy rate. For example, when $P^{\max} = 20$ dBm, the average system sum secrecy rate of DFAO method and PDDAPG method are 15.63 bits/s/Hz and 18.91 bits/s/Hz respectively. This means that compared with DFAO method, the proposed approach enhances the secrecy rate by approximately 21%. Moreover, the active RIS demonstrates significantly higher performance improvement than the passive RIS.

Fig. 4 shows the relationship between the average system sum secrecy rate and the number of RIS elements N. From the figure, it can be seen that with the increase of N, the secrecy rate under each scheme also increases. We also notice that in the active RIS-assisted system, the secrecy rate of PDDAPG method is higher than that of DFAO algorithm when N is greater than 25, and the greater the N, the more obvious the performance difference between the two algorithms. For instance, when N is increased from 25 to 100, the average secrecy rate realized by the PDDAPG method is increased from 14.33 bits/s/Hz to 21.94 bits/s/Hz (increase of 7.61 bps/Hz), and the average secrecy rate realized by DFAO method are increased from 14.33 bits/s/Hz to 15.78 bits/s/Hz (increase of 1.45 bits/s/Hz). It should be noted that in a practical system, N is hundreds, if not thousands [21]. Thus, in the active RIS-assisted system, PDDAPG method has better performance.

Fig. 5 shows the average run time comparison between the proposed PDDAPG method and the DFAO method. In Fig. 5, with the increase of N, the average run time under each scheme also increases. From Fig. 5 (a), it can be seen that different step size initial values have little impact on the average run time of the PDDAPG method. When the step size initial value is 0.01 (i.e., $\alpha^0 = \tau^0 = 0.01$), the average run time of the PDDAPG method can be reduced by approximately 76% compared to the DFAO algorithm. From Fig. 5 (b), it can be observed that different initial values of $\mathbf{x}$ and $\boldsymbol{\theta}$ also have no significant impact on the average run time of the PDDAPG algorithm. In conclusion, our proposed PDDAPG method is not sensitive to step size and initial points.

Fig. 6 depicts the impact of QoS and without QoS on the achievable secrecy rates for each Bob. As anticipated, the overall secrecy rates of the system increase with the increase of $P^{\max}$. This is because as $P^{\max}$ increases, Bob's received SINR improves, thereby enhancing performance.

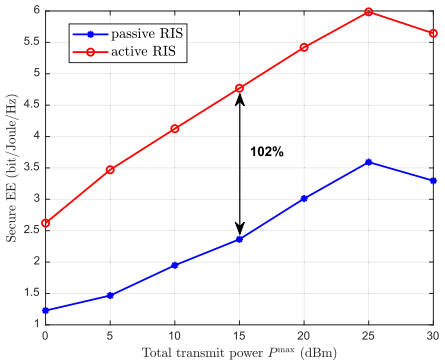

FIGURE 7. Secure EE comparison between active RIS and passive RIS.

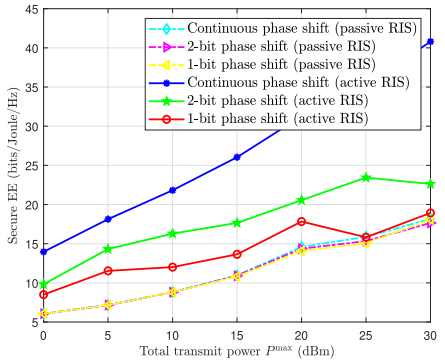

FIGURE 8. Secure EE comparison between continuous and discrete phase shift Cases.

Additionally, Compared to Fig. 6 (b), it can be observed that our proposed joint beamforming and precoding scheme results as illustrated in from Fig. 6 (a) achieves comparable secrecy rates for each Bob, ensuring fairness among users. This is attributed to the introduction of QoS constraints, which guarantees that the minimum secrecy rate for each Bob meets a certain level.

Fig. 7 illustrates the relationship between the secure EE and the total power consumption $P^{\max}$ of active RIS and passive RIS. From Fig. 7, it can be seen that the secure EE of active RIS increases by approximately 102% compared to passive RIS. Additionally, we also observed that as the total power consumption $P^{\max}$ increases, the secure EE first reaches a peak and then gradually decreases. This phenomenon can be explained by the fact that when $P^{\max}$ is relatively low, the rate of increase in secure EE is higher than the rate of increase in $P^{\max}$.

Fig. 8 shows that in the passive RIS scenario, the curves for "*Continuous phase shift*", "*2-bit phase shift*" and "*1-bit* phase shift" are very close. However, under the active RIS scenario, the 2-bit and 1-bit cases experience slight performance degradation. This is mainly because in the active RIS scenario, optimizing the amplitude plays a crucial role in improving secure energy efficiency. This suggests that relying solely on angle projection can lead to deviations from the optimal solution. In contrast, in the passive RIS scenario, where RIS elements have a constant amplitude of 1,

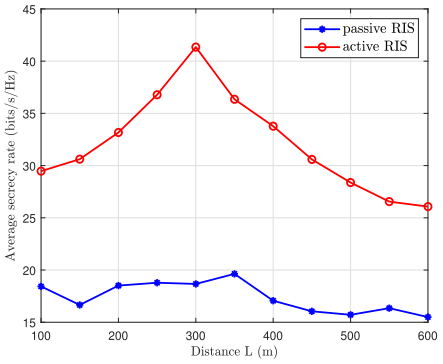

FIGURE 9. Secure EE comparison between continuous and discrete phase shift Cases.

the conversion from continuous phase shift to discrete phase shift introduces relatively small errors and results in lower performance degradation.

From Fig. 9, it can be observed that users deployed with active RIS achieve the highest secure rate at a coordinate position of 300 meters, which corresponds to the radius closest to the active RIS. This indicates that users at this distance radius can receive strong signals reflected by the active RIS. In contrast, users with passive RIS show lower sensitivity to coordinates. Although the highest secure rate is achieved at a coordinate of 350 meters, the performance improvement relative to other coordinates is moderate.

VII. CONCLUSION

In this paper, an active RIS-assisted multiuser MISO secure communication system is studied. We propose a PDDAPG method to solve the problem of SSR maximization. The simulation results show that the proposed PDDAGP method achieves a 21% increase in secrecy rate compared to the benchmark algorithm. Additionally, the active RIS-assisted scheme demonstrates better results in terms of secrecy rate. We also prove that the complexity of each iteration of the PDDGP method grows linearly with the number of reflecting elements at RIS. This complexity is much lower than existing methods, making it easy to apply in practice. To further satisfy different QoS requirements, a method based on FP and DC methods is proposed. The FP method reformulates the nonconvex capacity of legal users into a convex form, while the DC method addresses the nonconvex capacity of the eavesdropper through first-order Taylor approximations.

APPENDIX A PROOF OF LEMMA 2

For notational simplicity, we rewrite C_3 as

$$\left|\widetilde{\mathbf{H}}_{\mathrm{B},k}\mathbf{x}_k\right|^2 \geq \Big(\sum\nolimits_{j=1}^{K}\left|\widetilde{\mathbf{H}}_{\mathrm{B},k}x_j\right|^2 + \left\|\mathbf{H}_{\mathrm{IU},k}\mathbf{\Phi}\right\|^2\sigma_v^2+\sigma^2\Big)(1-2^{-\eta_k}), \tag{43}$$

Via Cauchy-Schwarz Inequality, we have

$$\sum_{j=1}^{K}\left|\widetilde{\mathbf{H}}_{\mathrm{B},k}x_j\right|^2 \le \left|\widetilde{\mathbf{H}}_{\mathrm{B},k}\right|^2\sum_{j=1}^{K}\left|x_j\right| \le \left|\widetilde{\mathbf{H}}_{\mathrm{B},k}\right|^2\sum_{j=1}^{K}P_{max} \tag{44}$$

Substitute (44) into (43, we have (27).

(43) still is nonconvex, we can utilize the Taylor approximation to reformulate the left term of (43)

$$\|\widetilde{\mathbf{H}}_{\mathrm{B},k}\mathbf{x}_k\|^2 \le 2\mathrm{Re}\{\widetilde{\mathbf{H}}_{\mathrm{B},k}\mathbf{x}_k\} - \|\widetilde{\mathbf{H}}_{\mathrm{B},k}\mathbf{x}_k^n\|^2, \tag{45}$$

then combining (43) we have

$$\begin{aligned}&2\mathrm{Re}\{\widetilde{\mathbf{H}}_{\mathrm{B},k}\mathbf{x}_k\} - \|\widetilde{\mathbf{H}}_{\mathrm{B},k}\mathbf{x}_k^n\|^2 \ge\\ &(\|\widetilde{\mathbf{H}}_{\mathrm{B},k}\|^2P_{\mathrm{BS}}^{\max} + \left\|\mathbf{H}_{\mathrm{IU},k}\Phi\right\|^2\sigma_v^2+\sigma)(1-2^{-\eta_k}).\end{aligned} \tag{46}$$

which completes the proof.

APPENDIX B PROOF OF LEMMA 3

Following the proof strategy of Lemma 2, we first reformulate C_4 as

$$\|\widetilde{\mathbf{H}}_{\mathrm{E}}\mathbf{x}_k\|^2 \le (\sum_{i\neq k}\{\|\widetilde{\mathbf{H}}_{\mathrm{E}}\mathbf{x}_i\|^2\} + \|\mathbf{H}_{\mathrm{IE}}\Phi\|^2\sigma_v^2+\sigma_e)(2^{\eta_{e,k}}-1) \tag{47}$$

By utilizing the Taylor approximation to reformulate the right first term of (47), we have

$$\|\widetilde{\mathbf{H}}_{\mathrm{E}}\mathbf{x}_i\|^2 \le \{2\mathrm{Re}\{\widetilde{\mathbf{H}}_{\mathrm{E}}\mathbf{x}_i\} - \|\widetilde{\mathbf{H}}_{\mathrm{E}}\mathbf{x}_i^n\|^2\}, \tag{48}$$

where $\mathbf{x}_i^n$ is the n-th iterative point. Combining (47), we have

$$\begin{aligned}\|\widetilde{\mathbf{H}}_{\mathrm{E}}\mathbf{x}_k\|^2 \le (&\sum_{i\neq k}\{2\mathrm{Re}\{\widetilde{\mathbf{H}}_{\mathrm{E}}\mathbf{x}_i\} - \|\widetilde{\mathbf{H}}_{\mathrm{E}}\mathbf{x}_i^n\|^2\}\\ &+ \|\mathbf{H}_{\mathrm{IE}}\Phi\|^2\sigma_v^2+\sigma_e)\times(2^{\eta_{e,k}}-1),\end{aligned} \tag{49}$$

which completes the proof.

ACKNOWLEDGMENT

(Bin Gao and Jingru Zhao contributed equally to this work.)

REFERENCES

[1] Z. Yang, W. Xu, C. Huang, J. Shi, and M. Shikh-Bahaei, "Beamforming design for multiuser transmission through reconfigurable intelligent surface," *IEEE Trans. Commun.*, vol. 69, no. 1, pp. 589–601, Jan. 2021.

[2] Q. Wu and R. Zhang, "Towards smart and reconfigurable environment: Intelligent reflecting surface aided wireless network," *IEEE Commun. Mag.*, vol. 58, no. 1, pp. 106–112, Jan. 2020.

[3] C. Huang, A. Zappone, G. C. Alexandropoulos, M. Debbah, and C. Yuen, "Reconfigurable intelligent surfaces for energy efficiency in wireless communication," *IEEE Trans. Wireless Commun.*, vol. 18, no. 8, pp. 4157–4170, Aug. 2019.

[4] Q. Wu and R. Zhang, "Intelligent reflecting surface enhanced wireless network via joint active and passive beamforming," *IEEE Trans. Wireless Commun.*, vol. 18, no. 11, pp. 5394–5409, Nov. 2019.

[5] L. Yang, J. Yang, W. Xie, M. O. Hasna, T. Tsiftsis, and M. D. Renzo, "Secrecy performance analysis of RIS-aided wireless communication systems," *IEEE Trans. Veh. Technol.*, vol. 69, no. 10, pp. 12296–12300, Oct. 2020.

[6] L. Wei, K. Wang, C. Pan, and M. Elkashlan, "Secrecy performance analysis of RIS-aided communication system with randomly flying eavesdroppers," *IEEE Wireless Commun. Lett.*, vol. 11, no. 10, pp. 2240–2244, Oct. 2022.

[7] M. Kaveh, Z. Yan, and R. Jäntti, "Secrecy performance analysis of RIS-aided smart grid communications," *IEEE Trans. Ind. Informat.*, vol. 20, no. 4, pp. 5415–5427, Apr. 2024.

[8] F. R. Ghadi and G. A. Hodtani, "Copula-based analysis of physical layer security performances over correlated Rayleigh fading channels," *IEEE Trans. Inf. Forensics Security*, vol. 16, pp. 431–440, 2021.

[9] J. Zhang, H. Du, Q. Sun, B. Ai, and D. W. K. Ng, "Physical layer security enhancement with reconfigurable intelligent surface-aided networks," *IEEE Trans. Inf. Forensics Security*, vol. 16, pp. 3480–3495, 2021.

[10] Z. Zhang, L. Dai, X. Chen, C. Liu, F. Yang, R. Schober, and H. V. Poor, "Active RIS vs. Passive RIS: Which will prevail in 6G?" *IEEE Trans. Commun.*, vol. 71, no. 3, pp. 1707–1725, Mar. 2023.

[11] A. Mukherjee, V. Kumar, and L.-N. Tran, "Secrecy rate maximization for intelligent reflecting surface assisted MIMOME wiretap channels," in *Proc. IEEE Mil. Commun. Conf.*, Nov. 2021, pp. 261–266.

[12] V. Kumar, M. F. Flanagan, D. W. Kwan Ng, and L.-N. Tran, "On the secrecy rate under statistical QoS provisioning for RIS-assisted MISO wiretap channel," in *Proc. IEEE Global Commun. Conf.*, Dec. 2021, pp. 1–6, doi: 10.1109/GLOBECOM46510.2021.9685957.

[13] Y. Ma, M. Li, Y. Liu, Q. Wu, and Q. Liu, "Optimization for reflection and transmission dual-functional active RIS-assisted systems," *IEEE Trans. Commun.*, vol. 79, no. 9, pp. 5534–5548, Sep. 2023.

[14] K. Zhi, C. Pan, H. Ren, K. K. Chai, and M. Elkashlan, "Active RIS versus passive RIS: Which is superior with the same power budget?" *IEEE Commun. Lett.*, vol. 26, no. 5, pp. 1150–1154, May 2022.

[15] H. Niu, Z. Lin, K. An, X. Liang, Y. Hu, D. Li, and G. Zheng, "Active RIS-assisted secure transmission for cognitive satellite terrestrial networks," *IEEE Trans. Veh. Technol.*, vol. 72, no. 2, pp. 2609–2614, Feb. 2023.

[16] K. Shen and W. Yu, "Fractional programming for communication systems—Part I: Power control and beamforming," *IEEE Trans. Signal Process.*, vol. 66, no. 10, pp. 2616–2630, May 2018.

[17] L. Dong, H.-M. Wang, and H. Xiao, "Secure cognitive radio communication via intelligent reflecting surface," *IEEE Trans. Commun.*, vol. 69, no. 7, pp. 4678–4690, Jul. 2021.

[18] Q. Shi and M. Hong, "Penalty dual decomposition method for nonsmooth nonconvex optimization—Part I: Algorithms and convergence analysis," *IEEE Trans. Signal Process.*, vol. 68, pp. 4108–4122, 2020.

[19] C. Pan, H. Ren, K. Wang, W. Xu, M. Elkashlan, A. Nallanathan, and L. Hanzo, "Multicell MIMO communications relying on intelligent reflecting surfaces," *IEEE Trans. Wireless Commun.*, vol. 19, no. 8, pp. 5218–5233, Aug. 2020.

[20] M. Grant and S. Boyd. (2012). *CVX: MATLAB Software for Disciplined Convex Programming, Version 2.0 Beta*. [Online]. Available: http://cvxr.com/cvx

[21] L. Dai, B. Wang, M. Wang, X. Yang, J. Tan, S. Bi, S. Xu, F. Yang, Z. Chen, M. D. Renzo, C.-B. Chae, and L. Hanzo, "Reconfigurable intelligent surface-based wireless communications: Antenna design, prototyping, and experimental results," *IEEE Access*, vol. 8, pp. 45913–45923, 2020.

[22] Z. Zhang and L. Dai, "A joint precoding framework for wideband reconfigurable intelligent surface-aided cell-free network," *IEEE Trans. Signal Process.*, vol. 69, pp. 4085–4101, 2021.

[23] J. Lončar, A. Grbic, and S. Hrabar, "Ultrathin active polarization-selective metasurface at X-band frequencies," *Phys. Rev. B*, vol. 100, no. 7, Aug. 2019, Art. no. 075131.

[24] J.-F. Bousquet, S. Magierowski, and G. G. Messier, "A 4-GHz active scatterer in 130-nm CMOS for phase sweep amplify-and-forward," *IEEE Trans. Circuits Syst. I, Reg. Papers*, vol. 59, no. 3, pp. 529–540, Mar. 2012.

[25] K. K. Kishor and S. V. Hum, "An amplifying reconfigurable reflectarray antenna," *IEEE Trans. Antennas Propag.*, vol. 60, no. 1, pp. 197–205, Jan. 2012.

[26] S. Zhang, S. Zhang, F. Gao, J. Ma, and O. A. Dobre, "Deep learning optimized sparse antenna activation for reconfigurable intelligent surface assisted communication," *IEEE Trans. Commun.*, vol. 69, no. 10, pp. 6691–6705, Oct. 2021.

[27] Q. Hu, Y. Liu, Y. Cai, G. Yu, and Z. Ding, "Joint deep reinforcement learning and unfolding: Beam selection and precoding for mmWave multiuser MIMO with lens arrays," *IEEE J. Sel. Areas Commun.*, vol. 39, no. 8, pp. 2289–2304, Aug. 2021.

[28] W. Wang, X. Chen, L. You, X. Yi, and X. Gao, "Artificial noise assisted secure massive MIMO transmission exploiting statistical CSI," *IEEE Commun. Lett.*, vol. 23, no. 12, pp. 2386–2389, Dec. 2019.

[29] O. Lavi and N. Shlezinger, "Learn to rapidly and robustly optimize hybrid precoding," *IEEE Trans. Commun.*, vol. 71, no. 10, pp. 5814–5830, Oct. 2023.

BIN GAO received the B.S. and Ph.D. degrees from the PLA University of Science and Technology, China, in 2003 and 2008, respectively. He is currently an Associate Professor with the Faculty of Computer and Software Engineering, Huaiyin Institute of Technology, Huaiyin, China. His current research interests include optimization algorithm, reinforcement learning, physical layer security, physical layer security, IRS-aided wireless communications, and UAV-aided communications. He serves as a Reviewer for IEEE JOURNAL OF SELECTED TOPICS IN SIGNAL PROCESSING, IEEE TRANSACTIONS ON INFORMATION FORENSICS AND SECURITY, *Journal of Optimization Theory and Applications*, and IEEE COMMUNICATIONS LETTERS.

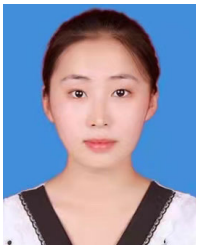

JINGRU ZHAO received the B.E. degree in computer science and technology from Qingdao University of Science and Technology, Shandong, China, in 2022. She is currently pursuing the master's degree with Huaiyin Institute of Technology, Jiangsu, China. Her current research interests include reconfigurable intelligent surface, deep learning, and future 6G networks.

SHIHAO YAN (Senior Member, IEEE) received the B.S. degree in communication engineering and the M.S. degree in communication and information systems from Shandong University, Jinan, China, in 2009 and 2012, respectively, and the Ph.D. degree in electrical engineering from the University of New South Wales (UNSW), Sydney, Australia, in 2015. He is currently a Senior Lecturer with the School of Science, Edith Cowan University (ECU), Perth, Australia. His current research interests include signal processing for wireless communication security and privacy, including covert communications, covert sensing, location spoofing detection, physical layer security, IRS-aided wireless communications, and UAV-aided communications. He was awarded the Humboldt Research Fellowship for experienced researchers and Australia Endeavour Research Fellowship. He was the Technical Co-Chair and a Panel Member of a number of IEEE conferences and workshops, including the IEEE GlobeCOM 2018 Workshop on Trusted Communications with Physical Layer Security and IEEE VTC 2017 Spring Workshop on Positioning Solutions for Cooperative ITS.

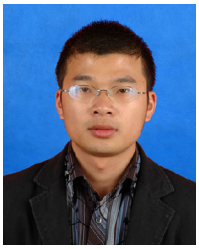

SHAOZHANG XIAO received the M.S. degree in computer science from the School of Jiangnan University, in 2012. He is currently a Senior Experimentalist with Huaiyin Institute of Technology. His research interests include the IoT technology, information hiding technology, and image processing.